Optimal pulse design for visible light positioning systems

Onurcan Yazar, Sinan Gezici*

Department of Electrical and Electronics Engineering, Bilkent University, Ankara 06800, Turkey

ABSTRACT

The problem of optimal pulse design for light-emitting diode (LED) transmitters is investigated in an indoor visible light positioning (VLP) setup. In particular, the problem of localization performance maximization is formulated for both asynchronous and synchronous VLP systems with consideration of practical limitations related to power consumption, illumination levels, and/or effective bandwidths, while quantifying the localization accuracy via the Cramér–Rao lower bound (CRLB). In both asynchronous and synchronous scenarios, the formulated problems are shown to be convex optimization problems, and some properties of the optimal solutions are derived. In addition, the pulse design problem for minimum power consumption is formulated under a CRLB constraint along with other practical limitations; and this problem is also revealed to be a convex optimization problem. Based on the solutions of the proposed optimization problems, pulse design procedures are described to determine the parameters of optimal pulse shapes. Numerical results illustrate the benefits of the proposed optimal pulse design approach in comparison with the state-of-the-art optimal power allocation scheme in the literature. In particular, electrical power consumption can be reduced by around 45% or localization accuracy can be improved by as much as 25% via the proposed optimal pulse design approach in certain scenarios.

© 2021 Elsevier B.V. All rights reserved.

1. Introduction

The usage of visible light systems with light-emitting diode (LED) transmitters for communications, particularly in indoor scenarios, is becoming an increasingly popular topic as visible light systems can provide high data rates, and serve multiple purposes of communication, indoor localization, sensing, and illumination without requiring additional infrastructure installation [1–3]. Short-range applications of visible light communication (VLC) have benefits in terms of power efficiency, communication security, cost, and license-free spectrum usage, and VLC is foreseen to become prevalent in upcoming generations of mobile technologies, e.g., sixth-generation (6G) [4–7]. Likewise, due to having less significant effects of multipath propagation in comparison with radio frequency (RF) based solutions, the visible light technology can facilitate realization of low-cost and accurate positioning systems in indoor environments. Therefore, visible light positioning (VLP) has attracted notable research interest recently and been investigated from various theoretical and practical perspectives in the literature [8–15,23].

In a typical VLP system, the main aim is to estimate the location (and orientation if unknown) of a VLC receiver, i.e., target node, by making use of the signals transmitted by several LED transmitters with known positions and orientations, which are also called anchor nodes. Numerous techniques available in the current literature regarding localization via visible light systems can be listed as received signal strength (RSS) [8], time of arrival (TOA) [9], time difference of arrival (TDOA) [10], angle of arrival (AOA) [11], phase difference of arrival (PDOA) [12], and hybrid (e.g., TDOA/RSS) schemes. Recent studies have focused on various aspects and applications of VLP systems. For example, in Majeed and Hranilovic [13], the performance limits of the maximum-likelihood (ML) location estimator and the Cramér–Rao lower bound (CRLB) on location estimation are considered for visible light-based passive indoor localization. The effects of exploiting multipath reflections as an information source in a VLP system are discussed in Hosseinianfar and Brandt-Pearce [14] through the analysis of the CRLB in various scenarios. Besides, a performance analysis of non-line-of-sight (NLOS) propagation in RSS-based VLP systems is carried out in Zhou et al. [15], by deriving closed-form CRLB expressions for target location and orientation estimation. Although photo detectors are commonly used at the receiver side of an VLP system, imaging sensors (cameras) can also be employed in various applications as they are already available in smart devices [16–19]. In [19,20], machine learning techniques are utilized for accurate localization in camera based visible light systems. For instance, an arti-

* Corresponding author.
E-mail addresses: onurcan@ee.bilkent.edu.tr (O. Yazar), gezici@ee.bilkent.edu.tr (S. Gezici).

ficial neural network (ANN) is used in Lin [20] for two-dimensional visible light positioning by grouping LEDs into blocks and encoding the block coordinates. In addition, Hsu [21], Chuang [22] focus on the application of machine learning algorithms for photo detector based VLP systems.

Optimal resource allocation methods have been thoroughly studied in the visible light communication and positioning (VLCP) literature. For example, in Keskin et al. [8], the optimal and robust power allocation schemes for LED transmitters are developed with the objective of maximizing localization performance under illumination constraints, where the localization performance is measured via the CRLB on location estimation. The study in Yazar et al. [23] examines a robust power allocation problem in VLP systems with the aim of minimum power consumption, in the presence of stochastic uncertainties in localization parameters, and measures the localization performance via the CRLB. The works in Bykhovsky and Arnon [24], Ling et al. [25] focus on optimal power allocation strategies for LED transmitters in a VLC system with the aim of maximizing the total transmission rate over subcarriers for orthogonal frequency-division multiplexing (OFDM) based communications. As an intelligent resource allocation technique for integrated VLCP systems, a model-free reinforcement learning based method is proposed in Yang [26]. The authors of Yang [27] consider multiuser VLCP configurations and come up with a joint subcarrier and power allocation approach to be implemented in such systems. Moreover, a coordinated resource allocation strategy that is realizable in indoor Internet-of-Things (IoT) scenarios is investigated in Yang [28].

Optimal resource allocation strategies have admitted significant research interest in the design of RF based localization systems, as well. For instance, in Garcia et al. [29], optimal joint allocation of power and bandwidth is performed with the aim of maximizing target localization accuracy in a multiple-input multiple-output radar network, where the localization performance is quantified via the CRLB. The work in Zhang et al. [30] investigates the joint power and spectrum allocation optimization in a resource-restricted wireless network localization setup by proposing approximate geometric programming formulations. A robust resource allocation problem for localization accuracy maximization and power consumption minimization in the presence of measurement uncertainties is examined in Li et al. [31] for a wireless localization system. Moreover, in Nowak [32], signal and system design for a multi-frequency localization system for increased energy efficiency is carried out, and the theoretical limits regarding the ranging accuracy are quantified via the CRLB.

Having the motivation of improvements manifested in recent studies on optimal power and resource allocation in localization networks, our goal in this paper is to design optimal pulse shapes for LED transmitters in asynchronous and synchronous VLP systems under practical constraints. More specifically, we formulate the optimal transmitted pulse design problem to improve localization accuracy, specified via the CRLB, under several system constraints regarding power restrictions in LEDs and illumination requirements over specified regions. We also perform a theoretical analysis of this problem for both asynchronous and synchronous VLP systems. In addition, we formulate the problem of optimal pulse design for minimum total power consumption in LED transmitters while guaranteeing a certain level of localization performance under practical system constraints. Moreover, we describe procedures for specifying the optimal parameters of pulse shapes based on the solutions of the proposed optimization problems. Although the optimal power allocation problem is investigated in Keskin et al. [8] based on similar power and illumination constraints, it employs only a single parameter, namely, the amplitudes, of pulse shapes for optimization. However, the localization accuracy not only depends on the amplitude (equivalently, the electrical

power) of pulses but also on their optical power and/or effective bandwidths. Therefore, via the optimal power allocation approach in Keskin et al. [8], optimal pulse shapes may not be attained. In this paper, we formulate the problem in terms of generic parameters related to transmitted pulses, which introduces more degrees of freedom in the design of pulses for each of the LED transmitters. The main contributions of this paper can be summarized as follows:

- For the first time in the literature, we formulate optimal pulse design problems for VLP systems under practical power and illumination constraints, where optical and electrical powers of LED transmitters are jointly optimized for asynchronous VLP systems, and optical and electrical powers of LED transmitters as well as effective bandwidths are jointly optimized for synchronous VLP systems. These generic formulations cover the optimal (electrical) power allocation approaches in Keskin et al. [8] as special cases.
- For both asynchronous and synchronous VLP systems, the problems of CRLB minimization under practical power and illumination constraints are shown to be convex problems. Also, some of the constraints are proved to hold with equality, which reduces the search space in the optimization problems.
- The problem of total (electrical) power minimization with a constraint on the CRLB under practical power and illumination constraints is formulated as a convex problem for both asynchronous and synchronous VLP systems.
- Explicit formulas are presented to specify the optimal parameters of pulse shapes based on the solutions of the proposed optimization problems. It is shown that improved localization accuracy and/or power efficiency can be attained since the same illumination constraints can be satisfied by consuming lower electrical power via the proposed approach than that in Keskin et al. [8].

In addition, various numerical examples are provided to evaluate performance of the proposed approaches in terms of the CRLB, the error of the ML estimator, and the total electrical power consumption considering a typical VLP setup, system parameters and constraints.

The remainder of this paper is organized as follows: Section 2 presents the VLP system model. In Section 3, the optimal pulse design problems are formulated for the minimization of the CRLB on localization and the minimization of the total power consumption in the LED transmitters by introducing the relevant system parameters and constraints. Also, the proposed optimization problems are analyzed theoretically. In Section 4, numerical results are presented and discussions on the advantages of the proposed optimal pulse design methodology are given. Finally, in Section 5, concluding remarks are made.

2. System model

We consider a VLP setup in which the aim is to estimate the location of a VLC receiver by utilizing the signals emitted by N_L LED transmitters. In this setup, only the line-of-sight (LOS) path between each LED transmitter and the VLC receiver is considered as in Armstrong et al. [1], Keskin et al. [8], Wang et al. [9], and it is assumed that the VLC receiver can process the signals sent by each of the LED transmitters separately (e.g., via code-division multiple access). Then, the received signal at the VLC receiver corresponding to the signal sent by the ith LED transmitter can be expressed as Wang et al. [9]

$$r_i(t) = \alpha_i R_p s_i(t - \tau_i) + \eta_i(t), \quad i = 1, \ldots, N_L \qquad (1)$$

for $t \in [T_{1,i}, \ T_{2,i}]$, where $T_{1,i}$ and $T_{2,i}$, respectively, represent the starting and ending time instants for the VLC receiver's observa-
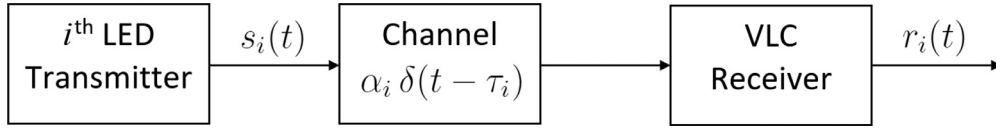
Fig. 1. System model involving the ith LED transmitter and the VLC receiver, where $i \in \{1, \ldots, N_L\}$. The optical signal $s_i(t)$ goes through the visible light channel with impulse response $\alpha_i \delta(t - \tau_i)$, and the channel output is converted to an electrical signal $r_i(t)$ by the photo detector at the VLC receiver as in (1).

tion of the signal transmitted by the ith LED transmitter, α_i denotes the optical channel attenuation factor between the ith LED transmitter and the VLC receiver ($\alpha_i > 0$), R_p is the photo detector responsivity of the VLC receiver, $s_i(t)$ is the signal transmitted by the ith LED transmitter, τ_i stands for the TOA of the signal arriving from the ith LED transmitter, and $\eta_i(t)$'s are independent zero-mean white Gaussian noise processes having spectral density level of σ^2 (please see Fig. 1).

The TOA parameter in (1) can be modeled as

$$\tau_i = \frac{\|\boldsymbol{l}_r - \boldsymbol{l}_t^i\|}{c} + \Delta_i, \quad i = 1, \ldots, N_L \tag{2}$$

where $\boldsymbol{l}_r = [l_{r,1}, l_{r,2}, l_{r,3}]^T$ and $\boldsymbol{l}_t^i = [l_{t,1}^i, l_{t,2}^i, l_{t,3}^i]^T$ denote the locations of the VLC receiver and the ith LED transmitter, respectively, c is the speed of light, $\|\cdot\|$ denotes the vector length operation, and Δ_i specifies the clock offset between the VLC receiver and the ith LED transmitter. The clock offsets $\{\Delta_i\}_{i=1}^{N_L}$ are modeled as deterministic unknown parameters for asynchronous VLP systems, whereas $\Delta_i = 0$, for $i = 1, \ldots, N_L$ refers to the synchronous VLP system case.

The channel attenuation factor α_i in (1) can be expressed through the Lambertian model as [33]

$$\alpha_i = \frac{(m_i + 1)S}{2\pi} \frac{[(\boldsymbol{l}_r - \boldsymbol{l}_t^i)^T \boldsymbol{n}_t^i]^{m_i} (\boldsymbol{l}_t^i - \boldsymbol{l}_r)^T \boldsymbol{n}_r}{\|\boldsymbol{l}_r - \boldsymbol{l}_t^i\|^{m_i+3}}, \quad i = 1, \ldots, N_L \tag{3}$$

where m_i is the Lambertian order for the ith LED transmitter, S is the area of the photo detector at the VLC receiver, and $\boldsymbol{n}_r = [n_{r,1}, n_{r,2}, n_{r,3}]^T$ and $\boldsymbol{n}_t^i = [n_{t,1}^i, n_{t,2}^i, n_{t,3}^i]^T$ denote the orientations of the VLC receiver and the ith LED transmitter, respectively.

In this setup, the VLC receiver is assumed to have the knowledge of some parameters such as $\boldsymbol{n}_r$ (which can be measured via a gyroscope), R_p, S, and $s_i(t)$, along with the parameters related to the LED transmitters, which can be gathered by communicating with each of the LED transmitters $\left(\text{i.e., } m_i, \boldsymbol{l}_t^i, \text{ and } \boldsymbol{n}_t^i, \text{ for } i \in \{1, \ldots, N_L\}\right)$ [8].

3. Optimal pulse design approaches

3.1. Assessment of localization accuracy

The localization accuracy of the VLP system can be quantified by the CRLB on the mean-squared error (MSE) of any unbiased location estimator ($\hat{\boldsymbol{l}}_r$) for the actual location of the VLC receiver ($\boldsymbol{l}_r$), which is stated as Poor [34], Keskin et al. [35]

$$\mathbb{E}\left\{\|\hat{\boldsymbol{l}}_r - \boldsymbol{l}_r\|^2\right\} \geq \text{trace}\left\{\mathbf{J}^{-1}\right\} \tag{4}$$

In (4), $\mathbf{J}$ represents the Fisher information matrix (FIM), which is computed differently for the asynchronous and synchronous VLP scenarios, due to having additional unknown parameters related to the clock time offsets (i.e., $\tau_1, \ldots, \tau_{N_L}$) in the asynchronous scenario. Namely, the FIM is given by $\mathbf{J} = \mathbf{J}_{asy}$ with the definition in (52) for asynchronous VLP systems, and by $\mathbf{J} = \mathbf{J}_{syn}$ with the definition in (53) for synchronous VLP systems (please see Appendix A).

The usage of CRLB as a performance metric can be justified by the fact that for sufficiently large signal-to-noise ratios (SNRs)

and/or effective bandwidths, the ML location estimator becomes asymptotically unbiased and efficient, i.e., its MSE converges to the CRLB [36,37]. Besides, the usage of CRLB facilitates mathematically tractable derivations.

In addition to other positioning parameters, the FIMs $\mathbf{J}_{asy}$ in (52) and $\mathbf{J}_{syn}$ in (53) depend on three sets of parameters related to the transmitted signals $s_i(t)$, namely, $E_1^{(i)}, E_2^{(i)}$, and $E_3^{(i)}$, which are defined as

$$E_1^{(i)} \triangleq \int_0^{T_{s,i}} \left(\frac{d}{dt} s_i(t)\right)^2 dt \tag{5}$$

$$E_2^{(i)} \triangleq \int_0^{T_{s,i}} \left(s_i(t)\right)^2 dt \tag{6}$$

$$E_3^{(i)} \triangleq \int_0^{T_{s,i}} s_i(t) \frac{d}{dt} s_i(t) dt \tag{7}$$

for $i \in \{1, \ldots, N_L\}$, where $T_{s,i}$ stands for the pulse width of $s_i(t)$. If the transmitted pulses are designed such that $s_i(0) = s_i(T_{s,i})$ is satisfied, which is a usual practice, then via (7), we have $E_3^{(i)} = 0$, for $i \in \{1, \ldots, N_L\}$.

3.2. System constraints

3.2.1. Individual electrical power limitations

Since the $E_2^{(i)}$ values in (6) are proportional to the electrical power of the ith LED transmitter, the constraint regarding the individual electrical power limitations can be expressed as Keskin et al. [8], Gong et al. [38]

$$\mathbf{E}_2^{lb} \preceq \mathbf{E}_2 \preceq \mathbf{E}_2^{ub} \tag{8}$$

with $\mathbf{E}_2 \triangleq [E_2^{(1)}, \ldots, E_2^{(N_L)}]^T$, where $\mathbf{E}_2^{lb}$ and $\mathbf{E}_2^{ub}$ stand for the lower and upper bounds on $\mathbf{E}_2$, respectively.

3.2.2. Total electrical power limitation

In many scenarios, the total power consumption in the LED transmitters is limited due to safety considerations or so as to stick to a power budget [8,33,39]. This constraint can be stated as

$$\mathbf{1}^T \mathbf{E}_2 \leq E_2^{tot} \tag{9}$$

with E_2^{tot} specifying the total electrical power limit for the LED transmitters.

3.2.3. Individual illuminance requirements

The horizontal illuminance generated at location $\mathbf{x}$ due to the ith LED is calculated as Keskin et al. [8], Gancarz et al. [39]

$$\mathcal{I}(\mathbf{x}, E_0^{(i)}) = E_0^{(i)} \phi_i(\mathbf{x}) \tag{10}$$

with

$$E_0^{(i)} \triangleq \int_0^{T_{s,i}} s_i(t) dt \tag{11}$$

and

$$\phi_i(\mathbf{x}) \triangleq \frac{(m_i + 1)\kappa_i}{2\pi T_{s,i}} \frac{[(\mathbf{x} - \boldsymbol{l}_t^i)^T \boldsymbol{n}_t^i]^{m_i} (l_{t,3}^i - x_3)}{\|\mathbf{x} - \boldsymbol{l}_t^i\|^{m_i+3}} \tag{12}$$

where κ_i denotes the luminous efficacy of the ith LED transmitter, for $i = 1, \ldots, N_L$. Then, the total illuminance produced at location $\mathbf{x}$ due to all the LEDs is found as Keskin et al. [8], Pandharipande and Caicedo [40]

$$\mathcal{I}_{\text{tot}}(\mathbf{x}, \mathbf{E}_0) = \sum_{i=1}^{N_L} \mathcal{I}(\mathbf{x}, E_0^{(i)}) = \sum_{i=1}^{N_L} E_0^{(i)} \phi_i(\mathbf{x}) = \boldsymbol{\phi}(\mathbf{x})^T \mathbf{E}_0 \quad (13)$$

with $\boldsymbol{\phi}(\mathbf{x})$ and $\mathbf{E}_0$ being defined as $\boldsymbol{\phi}(\mathbf{x}) \triangleq [\phi_1(\mathbf{x}), \ldots, \phi_{N_L}(\mathbf{x})]^T$ and $\mathbf{E}_0 \triangleq [E_0^{(1)}, \ldots, E_0^{(N_L)}]^T$, respectively. Then, the constraint regarding the individual illuminance requirements is stated as

$$\boldsymbol{\phi}(\mathbf{x}_\ell)^T \mathbf{E}_0 \geq \widetilde{\mathcal{I}}_\ell, \ \ell = 1, \ldots, L \quad (14)$$

where $\widetilde{\mathcal{I}}_\ell$ denotes the illuminance requirement for location $\mathbf{x}_\ell$ and L denotes the number of locations at which an illuminance requirement is specified.

3.2.4. Average illuminance requirement

From (10), the average illuminance over a region $\mathcal{A}$ is calculated as Keskin et al. [8]

$$\mathcal{I}_{\text{avg}}(\mathbf{E}_0) = \frac{1}{|\mathcal{A}|} \sum_{i=1}^{N_L} E_0^{(i)} \int_{\mathcal{A}} \phi_i(\mathbf{x}) \, d\mathbf{x} \quad (15)$$

with $|\mathcal{A}|$ denoting the volume of the region for which an average illuminance requirement is specified. Then, the corresponding constraint is stated as

$$\mathcal{I}_{\text{avg}}(\mathbf{E}_0) \geq \widetilde{\mathcal{I}}_{\text{avg}} \quad (16)$$

where $\widetilde{\mathcal{I}}_{\text{avg}}$ specifies the average illuminance requirement.

3.2.5. Jensen's inequality

Jensen's inequality for the transmitted signals $s_i(t)$ is stated as Poor [34]

$$\left(\frac{1}{T_{s,i}} \int_0^{T_{s,i}} s_i(t) \, dt \right)^2 \leq \frac{1}{T_{s,i}} \int_0^{T_{s,i}} \left(s_i(t) \right)^2 dt \quad (17)$$

for $i = 1, \ldots, N_L$. Via (6) and (11), this is equivalent to

$$\left(\frac{E_0^{(i)}}{T_{s,i}} \right)^2 \leq \frac{E_2^{(i)}}{T_{s,i}}, \ i = 1, \ldots, N_L \quad (18)$$

and can be stated as the constraint

$$\text{diag}\{\mathbf{E}_0\}\mathbf{E}_0 \preceq \text{diag}\{\mathbf{T}_s\}\mathbf{E}_2 \quad (19)$$

where $\text{diag}\{\cdot\}$ denotes the diagonalization operator[1] and $\mathbf{T}_s \triangleq [T_{s,1}, \ldots, T_{s,N_L}]^T$.

Although we consider design of signals $s_i(t)$'s in a generic form based on the parameters $E_0^{(i)}$, $E_1^{(i)}$, and $E_2^{(i)}$ in (5)–(7), these parameters cannot be selected arbitrarily, which could lead to non-realizable pulse shapes. To guarantee that the parameters lead to feasible pulse shapes, they must satisfy Jensen's inequality in (17). As long as $E_0^{(i)}$ and $E_2^{(i)}$ satisfy this inequality, the corresponding pulse shape can always be realized. Via Jensen's inequality, the relationship between electrical and optical powers is taken into account, and the transmitted signals (pulse shapes) are designed in a feasible manner.

3.2.6. Effective bandwidth limitation

Considering a synchronous VLP system, the effective bandwidth for the ith LED transmitter is expressed as

$$\beta^{(i)} = \sqrt{\frac{\int f^2 |S_i(f)|^2 \, df}{\int |S_i(f)|^2 \, df}} = \frac{1}{2\pi} \sqrt{E_1^{(i)}/E_2^{(i)}}, \ i = 1, \ldots, N_L \quad (20)$$

via Parseval's relation, where $S_i(f)$ denotes the Fourier transform of $s_i(t)$ [41]. Since the intensity of light cannot be changed in a very rapid manner due to hardware limitations, there exist upper limits on the effective bandwidths of the signals $s_i(t)$. Accordingly, the constraint regarding the LED transmitters' effective bandwidth limitation can be stated as

$$\mathbf{E}_1 \preceq 4\pi^2 \, \text{diag}\{\widetilde{\boldsymbol{\beta}}^{\text{ub}}\}\mathbf{E}_2 \quad (21)$$

where $\widetilde{\boldsymbol{\beta}}^{\text{ub}} \triangleq \left[(\beta^{\text{ub},(1)})^2, \ldots, (\beta^{\text{ub},(N_L)})^2 \right]^T$ specifies the upper bounds on the squares of the effective bandwidths for the LED transmitters.

Remark 1. The constraint in (19) is not considered in Keskin et al. [8] since only the amplitudes of pulse shapes are optimized in that work. For the same reason, the effective bandwidths are fixed in Keskin et al. [8], hence, (21) does not apply, either.

Remark 2. The following assumptions are made in the remainder of the paper:

(A1) Regarding the constraints in (8) and (9), $\mathbf{1}^T \mathbf{E}_2^{\text{lb}} \leq E_2^{\text{tot}}$ is assumed for the feasibility of the problems.
(A2) We assume that $E_2^{\text{tot}} \leq \mathbf{1}^T \mathbf{E}_2^{\text{ub}}$ holds in order to exclude the trivial solutions.
(A3) The FIMs are assumed to be positive definite (invertible) such that the CRLBs can be calculated.
(A4) It is assumed that $\widetilde{\boldsymbol{\alpha}}_i \neq \mathbf{0}$ for all $i = 1, \ldots, N_L$, where $\widetilde{\boldsymbol{\alpha}}_i \triangleq [\partial \alpha_i / \partial l_{r,1}, \partial \alpha_i / \partial l_{r,2}, \partial \alpha_i / \partial l_{r,3}]^T$ (please see the definition in (62)). This is a reasonable assumption since $\widetilde{\boldsymbol{\alpha}}_i = \mathbf{0}$ corresponds to an impractical scenario in which the received signal power (equivalently, RSS measurement) due to the ith LED does not provide any location information (e.g., please see (52)).[2]

3.3. CRLB minimization problems

The problems for maximizing the localization accuracy (i.e., minimizing the CRLB) are formulated for the asynchronous and synchronous cases separately since the optimization metrics and the constraints differ for each case.

3.3.1. Asynchronous case

Based on the constraints in (8), (9), (14), (16), and (19), the optimal pulse design problem for the maximization of the localization accuracy can be formulated in the asynchronous scenario as follows:

$$\underset{\mathbf{E}_0, \mathbf{E}_2}{\text{minimize}} \quad \text{trace}\left\{ \mathbf{J}_{\text{asy}}^{-1}(\mathbf{E}_2) \right\} \quad (22a)$$

$$\text{subject to} \quad \mathbf{E}_2^{\text{lb}} \preceq \mathbf{E}_2 \preceq \mathbf{E}_2^{\text{ub}} \quad (22b)$$

$$\mathbf{1}^T \mathbf{E}_2 \leq E_2^{\text{tot}} \quad (22c)$$

$$\boldsymbol{\phi}(\mathbf{x}_\ell)^T \mathbf{E}_0 \geq \widetilde{\mathcal{I}}_\ell, \ \ell = 1, \ldots, L \quad (22d)$$

---

[1] The diagonalization operator $\text{diag}\{\mathbf{x}\} : \mathbb{R}^{N \times 1} \to \mathbb{R}^{N \times N}$ returns a diagonal matrix $\mathbf{X}$, whose diagonal entries X_{ii} are equal to the input vector elements x_i, for $i = 1, \ldots, N$.

[2] Such a scenario can occur only when a VLC receiver and an LED transmitter cannot communicate, i.e., are not connected. Such an LED transmitter can be excluded from the list of LED transmitters for localization of the VLC receiver. Hence, this scenario can be omitted from the theoretical analysis without loss of generality.

$$\mathcal{I}_{\text{avg}}(\mathbf{E}_0) \geq \widetilde{\mathcal{I}}_{\text{avg}} \tag{22e}$$

$$\text{diag}\{\mathbf{E}_0\}\mathbf{E}_0 \preceq \text{diag}\{\mathbf{T}_s\}\mathbf{E}_2 \tag{22f}$$

It is noted that the lower limits in the illumination constraints in (22d) and (22e) can be determined by users depending on their specific needs. Compared to the formulation in Keskin et al. [8] where only the electrical powers of LED transmitters are optimized, the proposed formulation in (22) corresponds to the joint optimization of electrical and optical powers in the presence of the additional constraint in (22f) and achieves the overall optimal pulse design according to the CRLB metric. The price paid for the improved performance is the computational complexity since the dimensions of the optimization variables are N_L and $2N_L$ for the problems in Keskin et al. [8] and in this paper, respectively. However, the dimension increase may not be crucial in most practical systems since the problems are convex (please see Lemma 1 below) and they do not have to be solved very frequently (i.e., location updates are not very frequent in indoor localization systems).[3]

The reason for not considering the effective bandwidth constraint in (21) for the problem formulation in (22) can be explained as follows: The CRLB expression in (22a) does not depend on the $\mathbf{E}_1$ parameter in the asynchronous scenario (see (54)), which facilitates the use of sufficiently small values of $\mathbf{E}_1$ to satisfy any given set of effective bandwidth constraints (cf. Section 3.5). In other words, suppose that any arbitrary limits exist for the effective bandwidths in the system design. Then, some generic base signals (i.e., $\widetilde{s}_i(t)$'s in (38)) can be chosen in an appropriate manner to satisfy those limits, and then the scale and bias parameters of those base signals can be optimized to determine the optimal signal designs (see Section 3.5).

In the following lemma, the convexity of the problem in (22) is established.

Lemma 1. *The optimization problem in (22) is convex.*

Proof. The FIM for the asynchronous case is as expressed in (54) in Appendix A. Using the same argument as in Lemma 1 in Keskin et al. [8], we conclude that trace $\left\{\mathbf{J}_{\text{asy}}^{-1}(\mathbf{E}_2)\right\}$ is a convex function in $\mathbf{E}_2$; hence, the objective function in (22a) is convex. Besides, the constraints in (22b)–(22e) are linear (see (15)). In order to observe the convexity of the constraint in (22f), we can compute the Hessian matrix for the ith entry in the constraint as

$$\frac{2}{T_{s,i}^3(E_2^{(i)})^3} \begin{bmatrix} T_{s,i}^2(E_2^{(i)})^2 & -T_{s,i}E_0^{(i)}E_2^{(i)} \\ -T_{s,i}E_0^{(i)}E_2^{(i)} & (E_0^{(i)})^2 \end{bmatrix} \tag{23}$$

which is a positive semidefinite matrix. Therefore, the objective function of the problem in (22) is a convex function and its feasible set is a convex set. Thus, the problem in (22) is a convex optimization problem [42].∎

The following lemma states that the optimal pulse design parameters attain the total electrical power limit for the LED transmitters, i.e., (22c) is satisfied with equality when there exists a solution of (22) under the assumptions in Remark 2.

Lemma 2. *When the problem in (22) is feasible, its solution satisfies the inequality constraint in (22c) with equality.*

Proof. To prove the claim in the lemma via contradiction, suppose $\widehat{\mathbf{E}}_2$ is a solution of (22) with $\mathbf{1}^T\widehat{\mathbf{E}}_2 < E_2^{\text{tot}}$ (and satisfies all

the constraints). Since $E_2^{\text{tot}} \leq \mathbf{1}^T\mathbf{E}_2^{\text{ub}}$ is assumed to hold (please see (A2) in Remark 2), there exists a vector $\widetilde{\mathbf{E}}_2 = [\widetilde{E}_2^{(1)}, \ldots, \widetilde{E}_2^{(N_L)}]^T$ such that $\widetilde{E}_2^{(i)} = \widehat{E}_2^{(i)}$ for all $i \in \{1, \ldots, N_L\} \setminus \{j\}$ and $\widetilde{E}_2^{(j)} - \widehat{E}_2^{(j)} = \Delta > 0$. Here, Δ is chosen sufficiently small so as to satisfy both (22b) and (22c) for $\mathbf{E}_2 = \widetilde{\mathbf{E}}_2$. (The constraint in (22f) is satisfied automatically.)

From (52) in Appendix A (with $E_3^{(i)} = 0 \; \forall i$), the difference between the FIMs corresponding to $\widetilde{\mathbf{E}}_2$ and $\widehat{\mathbf{E}}_2$ can be computed as

$$\mathbf{J}_{\text{asy}}(\widetilde{\mathbf{E}}_2) - \mathbf{J}_{\text{asy}}(\widehat{\mathbf{E}}_2) = \frac{R_p^2 \Delta}{\sigma^2} \widetilde{\boldsymbol{\alpha}}_j \widetilde{\boldsymbol{\alpha}}_j^T \tag{24}$$

where j is the index for which $\widetilde{E}_2^{(j)} - \widehat{E}_2^{(j)} = \Delta$ and $\widetilde{\boldsymbol{\alpha}}_j \triangleq [\partial\alpha_j/\partial l_{r,1}, \partial\alpha_j/\partial l_{r,2}, \partial\alpha_j/\partial l_{r,3}]^T$. By invoking the Woodbury matrix inversion lemma [43], the following relations are obtained:

$$\mathbf{J}_{\text{asy}}^{-1}(\widetilde{\mathbf{E}}_2) = \left(\mathbf{J}_{\text{asy}}(\widehat{\mathbf{E}}_2) + \widetilde{\boldsymbol{\alpha}}_j \gamma \widetilde{\boldsymbol{\alpha}}_j^T\right)^{-1}$$

$$= \mathbf{J}_{\text{asy}}^{-1}(\widehat{\mathbf{E}}_2) - \mathbf{J}_{\text{asy}}^{-1}(\widehat{\mathbf{E}}_2)\widetilde{\boldsymbol{\alpha}}_j\left(\widetilde{\boldsymbol{\alpha}}_j^T\mathbf{J}_{\text{asy}}^{-1}(\widehat{\mathbf{E}}_2)\widetilde{\boldsymbol{\alpha}}_j + \frac{1}{\gamma}\right)^{-1}\widetilde{\boldsymbol{\alpha}}_j^T\mathbf{J}_{\text{asy}}^{-1}(\widehat{\mathbf{E}}_2)$$

$$= \mathbf{J}_{\text{asy}}^{-1}(\widehat{\mathbf{E}}_2) - \frac{1}{k}\mathbf{J}_{\text{asy}}^{-1}(\widehat{\mathbf{E}}_2)\widetilde{\boldsymbol{\alpha}}_j\widetilde{\boldsymbol{\alpha}}_j^T\mathbf{J}_{\text{asy}}^{-1}(\widehat{\mathbf{E}}_2) \tag{25}$$

where $\gamma \triangleq R_p^2\Delta/\sigma^2 > 0$ and $k \triangleq \widetilde{\boldsymbol{\alpha}}_j^T\mathbf{J}_{\text{asy}}^{-1}(\widehat{\mathbf{E}}_2)\widetilde{\boldsymbol{\alpha}}_j + 1/\gamma > 0$ due to the positive definiteness of $\mathbf{J}_{\text{asy}}(\widehat{\mathbf{E}}_2)$. Then, we have

$$\text{trace}\left\{\mathbf{J}_{\text{asy}}^{-1}(\widetilde{\mathbf{E}}_2)\right\} = \text{trace}\left\{\mathbf{J}_{\text{asy}}^{-1}(\widehat{\mathbf{E}}_2)\right\} - \frac{1}{k}\text{trace}\left\{\mathbf{J}_{\text{asy}}^{-1}(\widehat{\mathbf{E}}_2)\widetilde{\boldsymbol{\alpha}}_j\widetilde{\boldsymbol{\alpha}}_j^T\mathbf{J}_{\text{asy}}^{-1}(\widehat{\mathbf{E}}_2)\right\}$$

$$< \text{trace}\left\{\mathbf{J}_{\text{asy}}^{-1}(\widehat{\mathbf{E}}_2)\right\} \tag{26}$$

since $k > 0$ and trace$\left\{\mathbf{J}_{\text{asy}}^{-1}(\widehat{\mathbf{E}}_2)\widetilde{\boldsymbol{\alpha}}_j\widetilde{\boldsymbol{\alpha}}_j^T\mathbf{J}_{\text{asy}}^{-1}(\widehat{\mathbf{E}}_2)\right\} > 0$ due to the positive definiteness of $\mathbf{M}^T\mathbf{M}$ with $\mathbf{M} \triangleq \widetilde{\boldsymbol{\alpha}}_j^T\mathbf{J}_{\text{asy}}^{-1}(\widehat{\mathbf{E}}_2)$. (Note that $\widetilde{\boldsymbol{\alpha}}_j \neq \mathbf{0}$ due to assumption (A4) in Remark 2.) Hence, it is shown that $\widehat{\mathbf{E}}_2$ cannot be a solution of (22) since $\widetilde{\mathbf{E}}_2$ achieves a lower objective value and satisfies the constraints in (22).[4] This results in a contradiction to the initial assumption and implies that a feasible vector $\widehat{\mathbf{E}}_2$ with $\mathbf{1}^T\widehat{\mathbf{E}}_2 < E_2^{\text{tot}}$ cannot be a solution of (22) under the stated conditions. Therefore, solutions of (22) must satisfy the constraint in (22c) with equality.∎

Based on Lemma 2, the problem in (22) can be expressed as the following convex optimization problem:

$$\underset{\mathbf{E}_0, \mathbf{E}_2}{\text{minimize}} \qquad \text{trace}\left\{\mathbf{J}_{\text{asy}}^{-1}(\mathbf{E}_2)\right\} \tag{27a}$$

$$\text{subject to} \qquad \mathbf{E}_2^{\text{lb}} \preceq \mathbf{E}_2 \preceq \mathbf{E}_2^{\text{ub}} \tag{27b}$$

$$\mathbf{1}^T\mathbf{E}_2 = E_2^{\text{tot}} \tag{27c}$$

$$\boldsymbol{\phi}(\mathbf{x}_\ell)^T\mathbf{E}_0 \geq \widetilde{\mathcal{I}}_\ell, \; \ell = 1, \ldots, L \tag{27d}$$

$$\mathcal{I}_{\text{avg}}(\mathbf{E}_0) \geq \widetilde{\mathcal{I}}_{\text{avg}} \tag{27e}$$

$$\text{diag}\{\mathbf{E}_0\}\mathbf{E}_0 \preceq \text{diag}\{\mathbf{T}_s\}\mathbf{E}_2. \tag{27f}$$

where the inequality constraint in (22c) is replaced with the equality constraint in (27c), leading to a reduction in the search space.

---

[3] In the absence of illumination constraints, localization can performed even though the LEDs are conceived to be off by performing location updates occasionally.

[4] More generally, it is shown that the objective function in (22a) is a monotone decreasing function with respect to the elements of $\mathbf{E}_2$.

3.3.2. Synchronous case

Based on the constraints in (8), (9), (14), (16), (19), and (21), the optimal pulse design problem for the maximization of the localization accuracy can be formulated in the synchronous scenario as follows:

$$\underset{\mathbf{E}_0, \mathbf{E}_1, \mathbf{E}_2}{\text{minimize}} \quad \text{trace}\left\{\mathbf{J}_{\text{syn}}^{-1}(\mathbf{E}_1, \mathbf{E}_2)\right\} \tag{28a}$$

$$\text{subject to} \quad \mathbf{E}_2^{\text{lb}} \preceq \mathbf{E}_2 \preceq \mathbf{E}_2^{\text{ub}} \tag{28b}$$

$$\mathbf{1}^T \mathbf{E}_2 \leq E_2^{\text{tot}} \tag{28c}$$

$$\boldsymbol{\phi}(\mathbf{x}_\ell)^T \mathbf{E}_0 \geq \widetilde{\mathcal{I}}_\ell, \ \ell = 1, \ldots, L \tag{28d}$$

$$\mathcal{I}_{\text{avg}}(\mathbf{E}_0) \geq \widetilde{\mathcal{I}}_{\text{avg}} \tag{28e}$$

$$\text{diag}\{\mathbf{E}_0\}\mathbf{E}_0 \preceq \text{diag}\{\mathbf{T}_s\}\mathbf{E}_2 \tag{28f}$$

$$\mathbf{E}_1 \preceq 4\pi^2 \text{diag}\{\widetilde{\boldsymbol{\beta}}^{\text{ub}}\}\mathbf{E}_2 \tag{28g}$$

Compared to the formulation in Keskin et al. [8] where only the electrical powers of LED transmitters are optimized, the joint optimization over all the pulse parameters (equivalently, electrical powers, optical powers, and effective bandwidths) are performed in (28), leading to the overall optimal pulse design according to the CRLB metric.

In the following lemma, the convexity of the problem in (28) is stated.

Lemma 3. *The optimization problem in (28) is convex.*

Proof. Using a similar reasoning as in the proof of Lemma 1, we can show that the feasible set of (28) corresponds to a convex set. In order to show the convexity of the objective function, we define the parameter vector as $\boldsymbol{\theta} \triangleq \left[\mathbf{E}_1^T, \mathbf{E}_2^T\right]^T \in \mathbb{R}^{2N_{\text{L}}}$, and reexpress the objective function in (28a) as

$$f(\boldsymbol{\theta}) \triangleq \text{trace}\left\{\mathbf{J}_{\text{syn}}^{-1}(\mathbf{E}_1, \mathbf{E}_2)\right\}$$
$$= \text{trace}\left\{\left[(\mathbf{I}_3 \otimes \mathbf{E}_2)^T \boldsymbol{\Gamma} + (\mathbf{I}_3 \otimes \mathbf{E}_1)^T \widetilde{\boldsymbol{\Gamma}}\right]^{-1}\right\}. \tag{29}$$

where we employ the FIM expression for the synchronous case in (55) in Appendix A.

For any $\boldsymbol{\theta}^* = \left[\mathbf{E}_1^{*T}, \mathbf{E}_2^{*T}\right]^T \in \mathbb{R}^{2N_{\text{L}}}$, $\widetilde{\boldsymbol{\theta}} = [\widetilde{\mathbf{E}}_1^T, \widetilde{\mathbf{E}}_2^T]^T \in \mathbb{R}^{2N_{\text{L}}}$, and $\lambda \in [0, 1]$, we can obtain the following relations:

$$f(\lambda\boldsymbol{\theta}^* + (1-\lambda)\widetilde{\boldsymbol{\theta}}) = \text{trace}\left\{\left[(\mathbf{I}_3 \otimes (\lambda\mathbf{E}_2^* + (1-\lambda)\widetilde{\mathbf{E}}_2))^T \boldsymbol{\Gamma}\right.\right.$$
$$\left.\left. + (\mathbf{I}_3 \otimes (\lambda\mathbf{E}_1^* + (1-\lambda)\widetilde{\mathbf{E}}_1))^T \widetilde{\boldsymbol{\Gamma}}\right]^{-1}\right\}$$
$$\leq \lambda \, \text{trace}\left\{\left[(\mathbf{I}_3 \otimes \mathbf{E}_2^*)^T \boldsymbol{\Gamma} + (\mathbf{I}_3 \otimes \mathbf{E}_1^*)^T \widetilde{\boldsymbol{\Gamma}}\right]^{-1}\right\}$$
$$+ (1-\lambda) \, \text{trace}\left\{\left[(\mathbf{I}_3 \otimes \widetilde{\mathbf{E}}_2)^T \boldsymbol{\Gamma} + (\mathbf{I}_3 \otimes \widetilde{\mathbf{E}}_1)^T \widetilde{\boldsymbol{\Gamma}}\right]^{-1}\right\}$$
$$\leq \lambda f(\boldsymbol{\theta}^*) + (1-\lambda)f(\widetilde{\boldsymbol{\theta}}) \tag{30}$$

where we use the fact that $\text{trace}\{\mathbf{M}^{-1}\}$ is a convex function for $\mathbf{M} \succ 0$. The relation in (30) proves that the objective function is a convex function of $\boldsymbol{\theta}$, hence, of $\mathbf{E}_1$ and $\mathbf{E}_2$.

Since the feasible set of the problem in (28) is a convex set and the objective function is a convex function, the problem in (28) is a convex optimization problem. ■

The following lemma specifies the monotone decreasing nature of the objective function in (28a), which leads to the fact that the optimal pulse design parameters satisfy the inequality constraints in (28c) and (28g) with equality.

Lemma 4. *The objective function in (28a) is monotone decreasing with respect to $E_1^{(i)}$ and $E_2^{(i)}$, for all $i \in \{1, \ldots, N_{\text{L}}\}$, and the solution of the problem in (28), if feasible, satisfies (28c) and (28g) with equality.*

Proof. From (55) in Appendix A, the objective function of the problem in (28) can be expressed as $f(\mathbf{E}_1, \mathbf{E}_2) \triangleq \text{trace}\left\{\left[(\mathbf{I}_3 \otimes \mathbf{E}_2)^T \boldsymbol{\Gamma} + (\mathbf{I}_3 \otimes \mathbf{E}_1)^T \widetilde{\boldsymbol{\Gamma}}\right]^{-1}\right\}$. In order to show the monotonicity of this function with respect to the elements of $\mathbf{E}_1$, we define a new vector $\widetilde{\mathbf{E}}_1 = [\widetilde{E}_1^{(1)}, \ldots, \widetilde{E}_1^{(N_{\text{L}})}]^T$, where $\widetilde{E}_1^{(i)} = E_1^{(i)}$ for all $i \in \{1, \ldots, N_{\text{L}}\} \setminus \{j\}$ and $\widetilde{E}_1^{(j)} = E_1^{(j)} + \Delta$ for $\Delta > 0$. Then, the difference between the FIMs corresponding to $\widetilde{\mathbf{E}}_1$ and $\mathbf{E}_1$ can be found, via (53) (with $E_3^{(i)} = 0 \ \forall i$), as

$$\mathbf{J}_{\text{syn}}(\widetilde{\mathbf{E}}_1, \mathbf{E}_2) - \mathbf{J}_{\text{syn}}(\mathbf{E}_1, \mathbf{E}_2) = \frac{R_p^2 \alpha_j^2 \Delta}{\sigma^2} \widetilde{\boldsymbol{\tau}}_j \widetilde{\boldsymbol{\tau}}_j^T \tag{31}$$

with j is the index for which $\widetilde{E}_1^{(j)} - E_1^{(j)} = \Delta$ and $\widetilde{\boldsymbol{\tau}}_j \triangleq [\partial\tau_j/\partial l_{r,1}, \partial\tau_j/\partial l_{r,2}, \partial\tau_j/\partial l_{r,3}]^T$. Then, via the Woodbury matrix inversion lemma, we can show that

$$\mathbf{J}_{\text{syn}}^{-1}(\widetilde{\mathbf{E}}_1, \mathbf{E}_2)$$
$$= \left(\mathbf{J}_{\text{syn}}(\mathbf{E}_1, \mathbf{E}_2) + \widetilde{\boldsymbol{\tau}}_j \, \gamma \, \widetilde{\boldsymbol{\tau}}_j^T\right)^{-1}$$
$$= \mathbf{J}_{\text{syn}}^{-1}(\mathbf{E}_1, \mathbf{E}_2) - \mathbf{J}_{\text{syn}}^{-1}(\mathbf{E}_1, \mathbf{E}_2)\widetilde{\boldsymbol{\tau}}_j\left(\widetilde{\boldsymbol{\tau}}_j^T\mathbf{J}_{\text{syn}}^{-1}(\mathbf{E}_1, \mathbf{E}_2)\widetilde{\boldsymbol{\tau}}_j + \frac{1}{\gamma}\right)^{-1}\widetilde{\boldsymbol{\tau}}_j^T\mathbf{J}_{\text{syn}}^{-1}(\mathbf{E}_1, \mathbf{E}_2)$$
$$= \mathbf{J}_{\text{syn}}^{-1}(\mathbf{E}_1, \mathbf{E}_2) - \frac{1}{k}\mathbf{J}_{\text{syn}}^{-1}(\mathbf{E}_1, \mathbf{E}_2)\widetilde{\boldsymbol{\tau}}_j\widetilde{\boldsymbol{\tau}}_j^T\mathbf{J}_{\text{syn}}^{-1}(\mathbf{E}_1, \mathbf{E}_2) \tag{32}$$

with $\gamma \triangleq R_p^2 \alpha_j^2 \Delta/\sigma^2 > 0$ and $k \triangleq \widetilde{\boldsymbol{\tau}}_j^T\mathbf{J}_{\text{syn}}^{-1}(\mathbf{E}_1, \mathbf{E}_2)\widetilde{\boldsymbol{\tau}}_j + 1/\gamma > 0$, due to the positive definiteness of $\mathbf{J}_{\text{syn}}(\mathbf{E}_1, \mathbf{E}_2)$. Then, we have

$$\text{trace}\left\{\mathbf{J}_{\text{syn}}^{-1}(\widetilde{\mathbf{E}}_1, \mathbf{E}_2)\right\} = \text{trace}\left\{\mathbf{J}_{\text{syn}}^{-1}(\mathbf{E}_1, \mathbf{E}_2)\right\}$$
$$- \frac{1}{k}\text{trace}\left\{\mathbf{J}_{\text{syn}}^{-1}(\mathbf{E}_1, \mathbf{E}_2)\widetilde{\boldsymbol{\tau}}_j\widetilde{\boldsymbol{\tau}}_j^T\mathbf{J}_{\text{syn}}^{-1}(\mathbf{E}_1, \mathbf{E}_2)\right\}$$
$$< \text{trace}\left\{\mathbf{J}_{\text{syn}}^{-1}(\mathbf{E}_1, \mathbf{E}_2)\right\} \tag{33}$$

since $\text{trace}\left\{\mathbf{J}_{\text{syn}}^{-1}(\mathbf{E}_1, \mathbf{E}_2)\widetilde{\boldsymbol{\tau}}_j\widetilde{\boldsymbol{\tau}}_j^T\mathbf{J}_{\text{syn}}^{-1}(\mathbf{E}_1, \mathbf{E}_2)\right\} > 0$ due to the positive definiteness of $\mathbf{M}^T\mathbf{M}$, with $\mathbf{M} \triangleq \widetilde{\boldsymbol{\tau}}_j^T\mathbf{J}_{\text{syn}}^{-1}(\mathbf{E}_1, \mathbf{E}_2)$.[5] This establishes the monotone decreasing property of $f(\mathbf{E}_1, \mathbf{E}_2)$ with respect to the elements of $\mathbf{E}_1$.

Similarly, we can define $\widetilde{\mathbf{E}}_2 = [\widetilde{E}_2^{(1)}, \ldots, \widetilde{E}_2^{(N_{\text{L}})}]^T$, where $\widetilde{E}_2^{(i)} = E_2^{(i)}$ for all $i \in \{1, \ldots, N_{\text{L}}\} \setminus \{\ell\}$ and $\widetilde{E}_2^{(\ell)} = E_2^{(\ell)} + \Delta$ for $\Delta > 0$. Then, the difference between the FIMs corresponding to $\widetilde{\mathbf{E}}_2$ and $\mathbf{E}_2$ can be found, via (53) (with $E_3^{(i)} = 0 \ \forall i$), as

$$\mathbf{J}_{\text{syn}}(\mathbf{E}_1, \widetilde{\mathbf{E}}_2) - \mathbf{J}_{\text{syn}}(\mathbf{E}_1, \mathbf{E}_2) = \frac{R_p^2 \Delta}{\sigma^2} \widetilde{\boldsymbol{\alpha}}_\ell \widetilde{\boldsymbol{\alpha}}_\ell^T \tag{34}$$

with $\widetilde{\boldsymbol{\alpha}}_\ell \triangleq [\partial\alpha_\ell/\partial l_{r,1}, \partial\alpha_\ell/\partial l_{r,2}, \partial\alpha_\ell/\partial l_{r,3}]^T$. Following the same lines as in the proof of Lemma 2, we observe that $f(\mathbf{E}_1, \mathbf{E}_2)$ is a monotone decreasing function with respect to $\mathbf{E}_2$.

Overall, the objective function in (28a) is monotone decreasing with respect to the elements of $\mathbf{E}_1$ and $\mathbf{E}_2$. Therefore, if a vector $\mathbf{E}_2$ is feasible for (28) with $\mathbf{1}^T\mathbf{E}_2 < E_2^{\text{tot}}$, then the arguments in the proof of Lemma 2 can be invoked to show that we can construct another feasible vector that achieves a lower objective value. Hence, a vector $\mathbf{E}_2$ with $\mathbf{1}^T\mathbf{E}_2 < E_2^{\text{tot}}$ cannot be the solution of (28); i.e., (28c) must be satisfied with equality. Similarly, if a vector $\mathbf{E}_1$ is feasible for (28) with $\mathbf{E}_1 \prec 4\pi^2 \text{diag}\{\widetilde{\boldsymbol{\beta}}^{\text{ub}}\}\mathbf{E}_2$, then there exists another feasible vector $\widetilde{\mathbf{E}}_1 = [\widetilde{E}_1^{(1)}, \ldots, \widetilde{E}_1^{(N_{\text{L}})}]^T$, where $\widetilde{E}_1^{(i)} = E_1^{(i)}$ for all $i \in \{1, \ldots, N_{\text{L}}\} \setminus \{j\}$ and $\widetilde{E}_1^{(j)} = E_1^{(j)} + \Delta$ with a sufficiently small $\Delta > 0$. Due to the monotonicity of the objective function in

---

[5] Please note that $\widetilde{\boldsymbol{\tau}}_j \neq \mathbf{0}$ for each j since the VLC receiver cannot be at the same location as any of the LED transmitters (see (63)).

(28a) with respect to the elements of $\mathbf{E}_1$, $\widetilde{\mathbf{E}}_1$ achieves a lower objective function; hence, $\mathbf{E}_1$ cannot be a solution; i.e., solutions of (28c) must satisfy (28g) with equality.■

As Lemma 4 claims, solutions of the optimization problem in (28) satisfy the inequality constraints in (28c) and (28g) with equality. Hence, the problem in (28) can equivalently be expressed as the following convex optimization problem:

$$\underset{\mathbf{E}_0, \mathbf{E}_2}{\text{minimize}} \quad \text{trace}\{\mathbf{J}_{\text{syn}}^{-1}(4\pi^2 \text{diag}\{\widetilde{\boldsymbol{\beta}}^{\text{ub}}\}\mathbf{E}_2, \mathbf{E}_2)\} \tag{35a}$$

$$\text{subject to} \quad \mathbf{E}_2^{\text{lb}} \preceq \mathbf{E}_2 \preceq \mathbf{E}_2^{\text{ub}} \tag{35b}$$

$$\mathbf{1}^T \mathbf{E}_2 = E_2^{\text{tot}} \tag{35c}$$

$$\boldsymbol{\phi}(\mathbf{x}_\ell)^T \mathbf{E}_0 \geq \widetilde{\mathcal{I}}_\ell, \ \ell = 1, \dots, L \tag{35d}$$

$$\mathcal{I}_{\text{avg}}(\mathbf{E}_0) \geq \widetilde{\mathcal{I}}_{\text{avg}} \tag{35e}$$

$$\text{diag}\{\mathbf{E}_0\}\mathbf{E}_0 \preceq \text{diag}\{\mathbf{T}_s\}\mathbf{E}_2. \tag{35f}$$

where the equality condition for (28g) is used to express $\mathbf{E}_1$ in terms of $\mathbf{E}_2$, and (28c) is replaced with the equality constraint in (35c). Comparing the original problem in (28) and the equivalent problem in (35), it can be observed that the number of optimization variables is reduced by a factor of 2/3, namely, from $[\mathbf{E}_0^T, \mathbf{E}_1^T, \mathbf{E}_2^T]^T \in \mathbb{R}^{3N_L}$ to $[\mathbf{E}_0^T, \mathbf{E}_2^T]^T \in \mathbb{R}^{2N_L}$.

3.4. Total power minimization problems

The problem of ensuring minimum power consumption in LED transmitters in a VLP system can be examined in the presence of practical power and illumination constraints as in the problems presented in Section 3.3, with the addition of a requirement regarding the localization accuracy [8]. Using the CRLB as a metric for the localization error performance, the total power minimization problem can be investigated for asynchronous and synchronous cases as follows.

3.4.1. Asynchronous case

The total power minimization problem for an asynchronous VLP system can be formulated as

$$\underset{\mathbf{E}_0, \mathbf{E}_2}{\text{minimize}} \quad \mathbf{1}^T \mathbf{E}_2 \tag{36a}$$

$$\text{subject to} \quad \mathbf{E}_2^{\text{lb}} \preceq \mathbf{E}_2 \preceq \mathbf{E}_2^{\text{ub}} \tag{36b}$$

$$\boldsymbol{\phi}(\mathbf{x}_\ell)^T \mathbf{E}_0 \geq \widetilde{\mathcal{I}}_\ell, \ \ell = 1, \dots, L \tag{36c}$$

$$\mathcal{I}_{\text{avg}}(\mathbf{E}_0) \geq \widetilde{\mathcal{I}}_{\text{avg}} \tag{36d}$$

$$\text{diag}\{\mathbf{E}_0\}\mathbf{E}_0 \preceq \text{diag}\{\mathbf{T}_s\}\mathbf{E}_2 \tag{36e}$$

$$\text{trace}\left\{\mathbf{J}_{\text{asy}}^{-1}(\mathbf{E}_2)\right\} \leq \epsilon_{\text{asy}} \tag{36f}$$

where ϵ_{asy} stands for the maximum tolerable CRLB level for the localization of the VLC receiver in the asynchronous scenario. Using the fact that trace$\left\{\mathbf{J}_{\text{asy}}^{-1}(\mathbf{E}_2)\right\}$ is a convex function (Lemma 1), it is observed that the problem in (36) is a convex optimization problem.

3.4.2. Synchronous case

The total power minimization problem for a synchronous VLP system can be formulated as

$$\underset{\mathbf{E}_0, \mathbf{E}_1, \mathbf{E}_2}{\text{minimize}} \quad \mathbf{1}^T \mathbf{E}_2 \tag{37a}$$

$$\text{subject to} \quad \mathbf{E}_2^{\text{lb}} \preceq \mathbf{E}_2 \preceq \mathbf{E}_2^{\text{ub}} \tag{37b}$$

$$\boldsymbol{\phi}(\mathbf{x}_\ell)^T \mathbf{E}_0 \geq \widetilde{\mathcal{I}}_\ell, \ \ell = 1, \dots, L \tag{37c}$$

$$\mathcal{I}_{\text{avg}}(\mathbf{E}_0) \geq \widetilde{\mathcal{I}}_{\text{avg}} \tag{37d}$$

$$\text{diag}\{\mathbf{E}_0\}\mathbf{E}_0 \preceq \text{diag}\{\mathbf{T}_s\}\mathbf{E}_2 \tag{37e}$$

$$\mathbf{E}_1 \preceq 4\pi^2 \text{diag}\left\{\widetilde{\boldsymbol{\beta}}^{\text{ub}}\right\}\mathbf{E}_2 \tag{37f}$$

$$\text{trace}\left\{\mathbf{J}_{\text{syn}}^{-1}(\mathbf{E}_1, \mathbf{E}_2)\right\} \leq \epsilon_{\text{syn}} \tag{37g}$$

where ϵ_{syn} stands for the maximum tolerable CRLB level for the localization of the VLC receiver in the synchronous scenario. The problem in (37) is a convex optimization problem as well, since its constraints are linear or convex and its objective function is linear.

The proposed total power minimization problems in (36) and (37) provide a more generic approach than the total power minimization approach in Keskin et al. [8] where only the electrical powers of LED transmitters are optimized. Therefore, improved power efficiency can be achieved via the proposed formulations, as investigated in Section 4.

Remark 3. In the proposed optimization problems in Sections 3.3 and 3.4, it is assumed that the localization parameters are perfectly known. If the localization parameters are known with some uncertainty (i.e., in the presence of imperfect knowledge), the robust formulations of the proposed problems can be obtained similarly to those discussed in Keskin et al. [8] and Yazar et al. [23] in a straightforward manner.

3.5. Calculation of optimal pulse design parameters

In this part, the main aim is to come up with signal shapes that comply with the optimal values of $\mathbf{E}_0$, $\mathbf{E}_1$, and $\mathbf{E}_2$, namely, $\mathbf{E}_0^*$, $\mathbf{E}_1^*$, and $\mathbf{E}_2^*$, respectively, that are determined via the solutions of the aforementioned optimization problems. Let us choose the transmitted pulses as

$$s_i(t) = \sqrt{P_i} \widetilde{s}_i(t) + b_i, \ t \in [0, T_{s,i}] \tag{38}$$

for $i = 1, \dots, N_L$, where $\widetilde{s}_i(t)$ is a generic base signal, and $\{P_i\}_{i=1}^{N_L}$ and $\{b_i\}_{i=1}^{N_L}$, respectively, are the scale and bias terms. Here, we remark that our proposed approach to the problem in terms of more general parameters related to signals (i.e., $\mathbf{E}_0$, $\mathbf{E}_1$, and $\mathbf{E}_2$) facilitates design of transmit pulses with two and three degrees of freedom in the asynchronous and synchronous cases, respectively, contrary to the power allocation approach in Keskin et al. [8] employing only one design parameter for each pulse, namely, P_i.

Using the definitions in (5), (6), and (11) for the signal model in (38), we obtain the following relations:

$$E_0^{*(i)} = \sqrt{P_i} \widetilde{E}_0^{(i)} + b_i T_{s,i} \tag{39}$$

$$E_1^{*(i)} = P_i \widetilde{E}_1^{(i)} \tag{40}$$

Table 1

Simulation parameters.

Parameter	Value
Room dimensions	$10 \times 10 \times 5$ m
Number of LED transmitters, N_L	4
Location of LED #1, $\boldsymbol{l}_t^1$	$[1\ 1\ 5]^T$ m
Location of LED #2, $\boldsymbol{l}_t^2$	$[1\ 9\ 5]^T$ m
Location of LED #3, $\boldsymbol{l}_t^3$	$[9\ 1\ 5]^T$ m
Location of LED #4, $\boldsymbol{l}_t^4$	$[9\ 9\ 5]^T$ m
Orientation of LEDs, $\boldsymbol{n}_t^i$, $i = 1, 2, 3, 4$	$[0\ 0\ -1]^T$
Number of illumination constraints, L	4
Location of illumination constraint #1, $\mathbf{x}_1$	$[1\ 1\ 1]^T$ m
Location of illumination constraint #2, $\mathbf{x}_2$	$[1\ 9\ 1]^T$ m
Location of illumination constraint #3, $\mathbf{x}_3$	$[9\ 1\ 1]^T$ m
Location of illumination constraint #4, $\mathbf{x}_4$	$[9\ 9\ 1]^T$ m
Orientation of VLC receiver, $\boldsymbol{n}_r$	$[0.5\ 0\ 0.866]^T$
Photo detector responsivity, R_p	0.4 mA/mW
Area of photo detector, S	1 cm^2
Noise spectral density level, σ^2	1.3381×10^{-22} W/Hz
LED Lambertian order, m_i, $i = 1, 2, 3, 4$	1
LED luminous efficacy, κ_i, $i = 1, 2, 3, 4$	284 lm/W
Pulse width, $T_{s,i}$, $i = 1, 2, 3, 4$	1 μs
Min. LED optical power	5 W
Max. LED optical power	20 W

$$E_2^{*(i)} = P_i \widetilde{E}_2^{(i)} + 2b_i \sqrt{P_i} \widetilde{E}_0^{(i)} + b_i^2 T_{s,i} \qquad (41)$$

where $\widetilde{E}_0^{(i)} \triangleq \int_0^{T_{s,i}} \widetilde{s}_i(t)\,dt$, $\widetilde{E}_1^{(i)} \triangleq \int_0^{T_{s,i}} (d\widetilde{s}_i(t)/dt)^2\,dt$ and $\widetilde{E}_2^{(i)} \triangleq \int_0^{T_{s,i}} (\widetilde{s}_i(t))^2\,dt$ for $i = 1, \ldots, N_L$, and $E_k^{*(i)}$ denotes the ith component of $\mathbf{E}_k^*$ for $k = 0, 1, 2$ and $i = 1, \ldots, N_L$.

In the asynchronous scenario, for given optimal values $\mathbf{E}_0^*$ and $\mathbf{E}_2^*$, the optimal pulse design parameters can be calculated from (39) to (41) as

$$P_i = \frac{E_2^{*(i)} T_{s,i} - (E_0^{*(i)})^2}{\widetilde{E}_2^{(i)} T_{s,i} - (\widetilde{E}_0^{(i)})^2} \qquad (42)$$

$$b_i = \frac{1}{T_{s,i}} \left(E_0^{*(i)} - \widetilde{E}_0^{(i)} \sqrt{\frac{E_2^{*(i)} T_{s,i} - (E_0^{*(i)})^2}{\widetilde{E}_2^{(i)} T_{s,i} - (\widetilde{E}_0^{(i)})^2}} \right) \qquad (43)$$

for $i = 1, \ldots, N_L$, considering any given set of base signals.

In the synchronous scenario, as the optimal values of $\mathbf{E}_0^*$, $\mathbf{E}_1^*$ and $\mathbf{E}_2^*$ are specified, we require an additional pulse design parameter to adjust the effective bandwidth $\widetilde{B}_i$ of the ith base signal $\widetilde{s}_i(t)$, which is computed as

$$\widetilde{B}_i = \frac{1}{2\pi} \sqrt{\widetilde{E}_1^{(i)} / \widetilde{E}_2^{(i)}}, \ i = 1, \ldots, N_L \qquad (44)$$

Then, for given $\mathbf{E}_0^*$, $\mathbf{E}_1^*$ and $\mathbf{E}_2^*$, this pulse design parameter is determined via (40) and (44) as

$$\widetilde{B}_i = \frac{1}{2\pi} \sqrt{\frac{E_1^{*(i)} (\widetilde{E}_2^{(i)} T_{s,i} - (\widetilde{E}_0^{(i)})^2)}{\widetilde{E}_2^{(i)} (E_2^{*(i)} T_{s,i} - (E_0^{*(i)})^2)}} \qquad (45)$$

for $i = 1, \ldots, N_L$, while the other pulse design parameters P_i and b_i are found via (42) and (43), respectively.

4. Numerical results

In this section, we present numerical results that illustrate the performance of the proposed optimal pulse design methodology for the problems of CRLB minimization and total power minimization. We simulate a VLP setup with parameters as given in Table 1 [8] and compare the results of the proposed approaches with the uniform and optimal power allocation strategies specified in Keskin

et al. [8].[6] We also consider the uniform electrical power distribution scheme which refers to $E_2^{(i)} = E_2^{tot}/N_L$, for $i = 1, \ldots, N_L$, subject to (22b)–(22f) as another baseline to evaluate the outcomes. This approach is labeled as "Pulse design (uniform)" in the figures. For solving the optimization problems in (27), (35), (36), and (37), the fmincon function of MATLAB is used with the interior-point algorithm.

In order to be in accordance with the work in Keskin et al. [8], we choose our base signals as

$$\widetilde{s}_i(t) = \frac{2}{3} \big(1 - \cos(2\pi t/T_{s,i})\big)\big(1 + \cos(2\pi f_{c,i}t)\big), \ t \in [0, T_{s,i}] \quad (46)$$

Then, the parameters of the base signals appearing in (39)–(41) can be expressed as

$$\widetilde{E}_0^{(i)} = \frac{2}{3} \left(T_{s,i} + \int_0^{T_{s,i}} \cos(2\pi f_{c,i}t)(1 - \cos(2\pi t/T_{s,i}))\,dt \right) \qquad (47)$$

$$\widetilde{E}_1^{(i)} = \frac{16\pi^2}{9} \int_0^{T_{s,i}} \left(\frac{\sin(2\pi t/T_{s,i})}{T_{s,i}} \big(1 + \cos(2\pi f_{c,i}t)\big) \right.$$
$$\left. - f_{c,i} \sin(2\pi f_{c,i}t)\big(1 - \cos(2\pi t/T_{s,i})\big) \right)^2 dt \qquad (48)$$

$$\widetilde{E}_2^{(i)} = \frac{4}{9} \int_0^{T_{s,i}} \big(1 - \cos(2\pi t/T_{s,i})\big)^2 \big(1 + \cos(2\pi f_{c,i}t)\big)^2\,dt \qquad (49)$$

In the asynchronous scenario, for the obtained optimal values of $\mathbf{E}_0$ and $\mathbf{E}_2$ (i.e., $\mathbf{E}_0^*$ and $\mathbf{E}_2^*$, respectively), the signal design parameters, P_i and b_i, can be determined from (42) and (43) based on the values in (47) and (49), where $f_{c,i}$'s can be set to any desired values without affecting the optimality (as they can be considered as free parameters in the asynchronous case). For simplicity, when we set $f_{c,i}$'s to integer multiples of $1/T_{s,i}$ except for $1/T_{s,i}$ or $2/T_{s,i}$, (47) and (49) reduce to $\widetilde{E}_0^{(i)} = 2T_{s,i}/3$ and $\widetilde{E}_2^{(i)} = T_{s,i}$, respectively. On the other hand, for the synchronous scenario, in the light of the discussion in Section 3.5, we regard $f_{c,i}$'s as design parameters, which modify the bandwidths of $\widetilde{s}_i(t)$'s. In this case, for the obtained optimal values of $\mathbf{E}_0$, $\mathbf{E}_1$, and $\mathbf{E}_2$ (i.e., $\mathbf{E}_0^*$, $\mathbf{E}_1^*$, and $\mathbf{E}_2^*$, respectively), the signal design parameters, P_i, b_i, and $f_{c,i}$, are determined from (40), (42), and (43) via (47)–(49).

In the numerical experiments, we first investigate the CRLB minimization problem for both the asynchronous and synchronous VLP scenarios under the VLP system constraints related to power consumption and ambient illumination levels. The optimal CRLB levels achieved by the solution of the asynchronous CRLB minimization problem in (27) versus different levels of average electrical power consumption are illustrated in Fig. 2 (labeled as "Pulse design (optimal)") for various VLC receiver locations and various illumination limits, together with the other methods; namely, the optimal and uniform power allocation algorithms in Keskin et al. [8], and the uniform pulse design approach. (The square-root of the objective function in (22a) achieved by each approach is presented in the y axes.) It can be observed from the figures that the introduction of a second degree of freedom on the transmit pulse design leads to improved performance in terms of the CRLB for relatively low values of total available power. Moreover, the proposed approach yields a feasible solution even for lower total power limits where the optimal power allocation approach in Keskin et al. [8] is not feasible for given illumination level requirements. The main reason why the proposed approach can ensure feasibility at a lower total electrical power than the existing approach is related to

---

[6] As in Keskin et al. [8], we calculate the average illuminance in (15) over the horizontal plane of the room at a fixed height of 1 m and also convert the LED optical power limits in Table 1 to individual electrical power limits in (8) by scaling their squares with $9T_s/4$ Keskin et al. [8, Sec. VII-A].
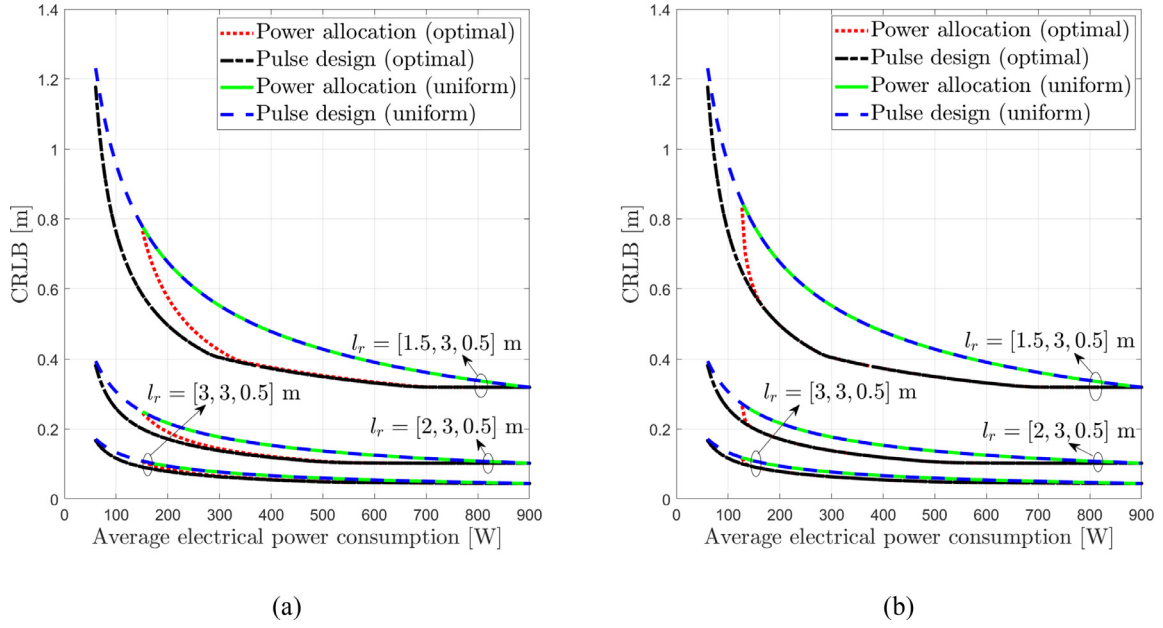
Fig. 2. CRLB on the MSE of location estimator versus average power consumption on LEDs in asynchronous scenario for different receiver locations and different illuminance requirements $(\widetilde{\mathcal{I}}_\ell, \widetilde{\mathcal{I}}_{\mathrm{avg}})$ (a) $(\widetilde{\mathcal{I}}_\ell, \widetilde{\mathcal{I}}_{\mathrm{avg}}) = (50, 10)$ lx and (b) $(\widetilde{\mathcal{I}}_\ell, \widetilde{\mathcal{I}}_{\mathrm{avg}}) = (30, 30)$ lx for $\ell = 1, 2, 3, 4$.
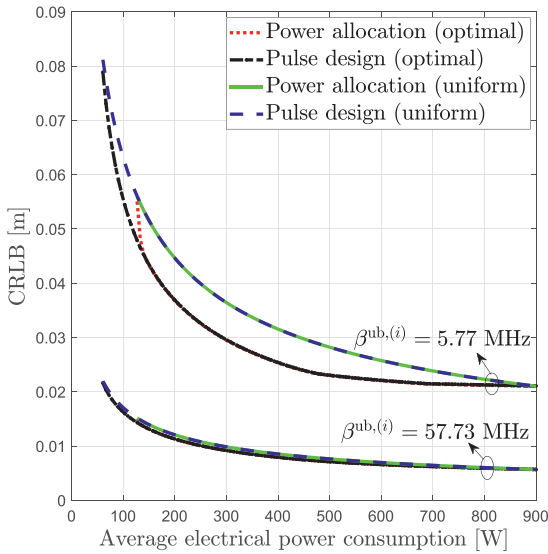
Fig. 3. CRLB on the MSE of location estimator versus average power consumption on LEDs in synchronous scenario for different effective bandwidths $\beta^{\mathrm{ub},(i)} = 5.77$ or 57.73 MHz for $i = 1, 2, 3, 4$, receiver location $\boldsymbol{l}_{\mathrm{r}} = [3, 3, 0.5]$ m, and illuminance requirement $\widetilde{\mathcal{I}}_\ell = \widetilde{\mathcal{I}}_{\mathrm{avg}} = 30$ lx for $\ell = 1, 2, 3, 4$.
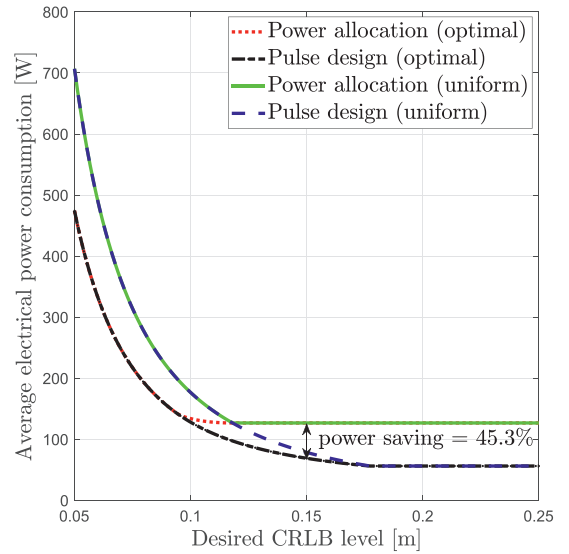
Fig. 4. Average power consumption on LEDs in asynchronous scenario for receiver location $\boldsymbol{l}_{\mathrm{r}} = [3, 3, 0.5]$ m and illuminance requirement $\widetilde{\mathcal{I}}_\ell = \widetilde{\mathcal{I}}_{\mathrm{avg}} = 30$ lx for $\ell = 1, 2, 3, 4$.

the flexibility of adjusting the $\mathbf{E}_0$ and $\mathbf{E}_2$ parameters (equivalently, the scale and bias terms) in the proposed pulse design approach. On the other hand, only the amplitudes of the pulse shapes are controlled in the optimal power allocation approach in Keskin et al. [8]. It is also noted from Fig. 2 that the significance of the performance improvements provided by the proposed approach depends on the location of the VLC receiver. Furthermore, the performance of the uniform pulse design (power allocation) can asymptotically approach that of the optimal pulse design (power allocation) at high average electrical power consumption since the electrical powers of all the signals reach the upper limit on the individual electrical powers.

The CRLB performance in the synchronous VLP scenario, which is obtained through the solution of the synchronous CRLB mini-

mization problem described in (35), is also investigated for two different effective bandwidth limitations, as illustrated in Fig. 3. Related to the statement in Lemma 4 about the attainment of the upper bound on the effective bandwidth to obtain the optimal CRLB, it is noted that the usage of a higher bandwidth results in lower CRLB levels. Besides, the same observations regarding the wider feasibility region and the lower CRLB values for the proposed approach than those in Keskin et al. [8] can be made as in the asynchronous case. Moreover, it is noted that the algorithms achieve very close performance for high effective bandwidths.

Example values for the optimal pulse design parameters for the asynchronous and synchronous scenarios corresponding to the proposed pulse design approach as well as to that in Keskin et al. [8] are shown in Tables 2 and 3, respectively. The values in the tables illustrate the flexibility provided by the proposed pulse de-
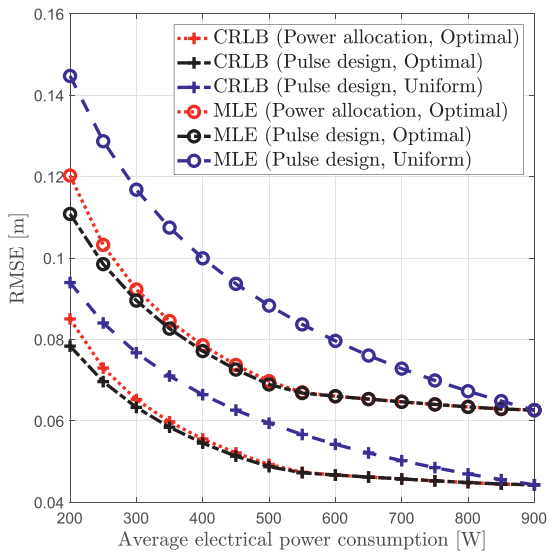
Table 2

Sample pulse design parameters for an asynchronous VLP setup with $\widetilde{\mathcal{I}}_\ell = 50$ lx for $\ell = 1, 2, 3, 4$, $\widetilde{\mathcal{I}}_{\text{avg}} = 10$ lx, and receiver location $\boldsymbol{l}_r = [3, 3, 0.5]$ m.

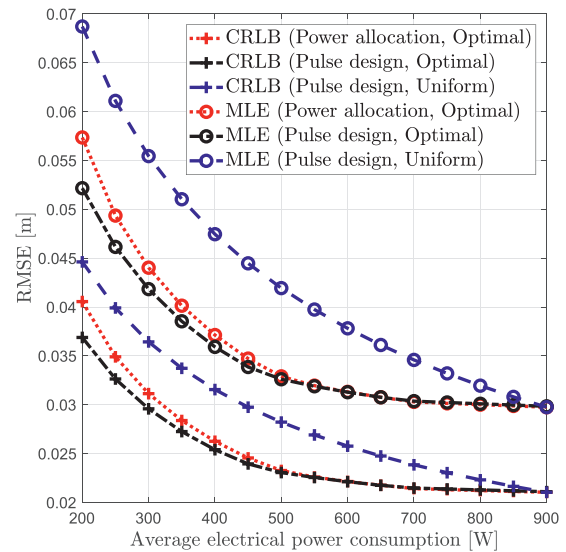| Average electrical power limit	100 W	250 W	400 W
P_1, P_2, P_3, P_4 (proposed)	2.143, 27.29, 23.56, 1.967	35.08, 185.2, 157.2, 6.042	86.4, 405.7, 341, 15.83
b_1, b_2, b_3, b_4 (proposed)	6.97, 7.97, 7.35, 7.01	4.79, 9.91, 8.77, 5.89	4.21, 9.58, 8.49, 4.95
P_1, P_2, P_3, P_4 (in Keskin et al. [8])	infeasible	143.71, 386.04, 328.2, 142.04	147.41, 728.1, 601.16, 123.32
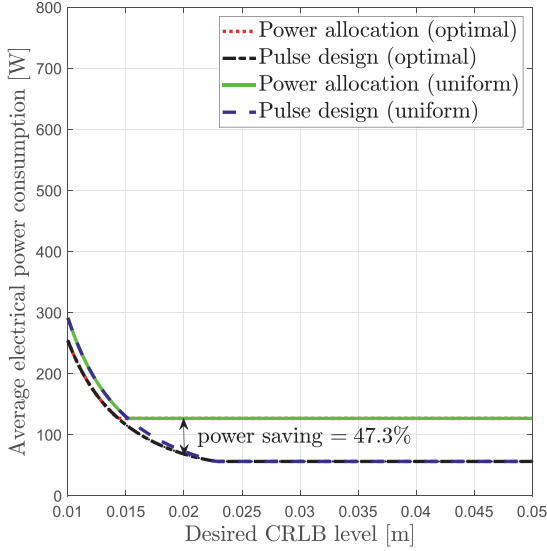
Fig. 5. Average power consumption on LEDs in synchronous scenario for receiver location $\boldsymbol{l}_r = [3, 3, 0.5]$ m, illuminance requirement $\widetilde{\mathcal{I}}_\ell = \widetilde{\mathcal{I}}_{\text{avg}} = 30$ lx for $\ell = 1, 2, 3, 4$, and effective bandwidth limitation $\beta^{\text{ub.}(i)} = 57.73$ MHz for $i = 1, 2, 3, 4$.

sign approach. For example, in the asynchronous case in Table 2, the proposed optimal approach can optimize both P_i and b_i in (38) whereas the optimal power allocation approach in Keskin et al. [8] can adjust P_i only (i.e., sets $b_i = 0$).

Next, the total power minimization problem is examined for asynchronous and synchronous VLP configurations. For the asynchronous scenario, the solution of the minimum power consumption problem in (36) is demonstrated as in Fig. 4. It is observed that the optimal pulse design approach achieves a lower total electrical power consumption than the optimal power allocation approach and the uniform power allocation approach for a range of desired CRLB levels. In Fig. 5, the minimum power consumption levels for the synchronous scenario, obtained through the solution of the problem in (37), is illustrated. We can observe that in the proposed approach, the LEDs require lower electrical powers in order to satisfy the desired CRLB levels than the other approaches, and power savings can be around 50% when the required CRLB level is not very low.

Finally, to evaluate the benefits of the proposed approach for practical estimators, we implement the ML estimators for $\boldsymbol{l}_r$ in the synchronous and asynchronous scenarios, named $\hat{\boldsymbol{l}}_r^{\text{syn}}$ and $\hat{\boldsymbol{l}}_r^{\text{asy}}$, respectively, which can be obtained as Keskin et al. [35]

$$\hat{\boldsymbol{l}}_r^{\text{syn}} = \arg\max_{\boldsymbol{l}_r} \sum_{i=1}^{N_L} \left(\alpha_i \int_{T_{1,i}}^{T_{2,i}} r_i(t) s_i(t - \tau_i) \, dt - 0.5 R_p \alpha_i^2 E_2^{(i)} \right) \quad (50)$$

and

$$\hat{\boldsymbol{l}}_r^{\text{asy}} = \arg\max_{\boldsymbol{l}_r} \sum_{i=1}^{N_L} \left(\alpha_i \widetilde{C}_{rs}^i - 0.5 R_p \alpha_i^2 E_2^{(i)} \right) \quad (51)$$

where $\widetilde{C}_{rs}^i \triangleq \int_{T_{1,i}}^{T_{2,i}} r_i(t) s_i(t - \hat{\tau}_i) \, dt$ and $\hat{\tau}_i$ is the ML estimate of τ_i, namely, $\hat{\tau}_i = \arg\max_{\tau_i} \int_{T_{1,i}}^{T_{2,i}} r_i(t) s_i(t - \tau_i) \, dt$. Based on the signal parameters obtained for different approaches, the root MSE (RMSE)

(a)

(b)

Fig. 6. RMSEs of ML estimators (MLEs) and CRLB values (in meters) for different approaches versus average power consumption on LEDs for receiver location $\boldsymbol{l}_r = [3, 3, 0.5]$ m, and illumination requirements $\widetilde{\mathcal{I}}_\ell = 50$ lx, $\widetilde{\mathcal{I}}_{\text{avg}} = 10$ lx for $\ell = 1, 2, 3, 4$, (a) for asynchronous scenario and (b) for synchronous scenario with effective bandwidth limitation $\beta^{\text{ub.}(i)} = 5.77$ MHz for $i = 1, 2, 3, 4$.

Table 3
Sample pulse design parameters for a synchronous VLP setup with $\widetilde{\mathcal{I}}_\ell = 50$ lx for $\ell = 1, 2, 3, 4$, $\widetilde{\mathcal{I}}_{avg} = 10$ lx, $\beta^{ub,(i)} = 5.77$ MHz for $i = 1, 2, 3, 4$, and receiver location $\boldsymbol{l}_r = [3, 3, 0.5]$ m.

Average electrical power limit	100 W	250 W	400 W
P_1, P_2, P_3, P_4 (proposed)	3.24, 0.116, 2.069, 0.0745	272.1, 23.45, 183.7, 13.78	258.2, 5.628, 174.2, 3.489
b_1, b_2, b_3, b_4 (proposed)	11.6, 7.669, 9.401, 7.782	7.463, 5.285, 6.65, 5.694	16.04, 5.849, 14.19, 6.193
$f_{c,1}, f_{c,2}, f_{c,3}, f_{c,4}$ [MHz](proposed)	71.45, 232.1, 72.36, 291.7	13.4, 19.06, 13.72, 23.2	18.2, 32.16, 18.91, 40.48
P_1, P_2, P_3, P_4 (in Keskin et al. [8])	infeasible	432.2, 138.6, 288.1, 141.1	737.5, 170.2, 539.2, 153.2

values for the ML estimators (MLEs) together with the CRLB values are presented in Fig. 6 for the asynchronous and synchronous scenarios. The results justify the legitimacy of the CRLB as a performance metric for the considered problem and indicate that the proposed optimal pulse design approach can provide lower RMSEs than the alternative methodologies. It is also noted that the ML estimators cannot converge to the CRLBs due to the presence of upper limits on the individual electrical powers of the LED transmitters.

5. Concluding remarks

In this paper, we proposed the approach of optimal pulse shape design for LED transmitters in asynchronous and synchronous VLP systems with the objective of improved localization performance under several system constraints regarding LED powers and illumination levels. In addition, we formulated the problem of optimal pulse design for minimum total power consumption in LEDs under a certain requirement on the localization performance. All the proposed optimization problems were proved to be convex; hence they can be solved efficiently via standard convex optimization tools. In addition, some of the inequality constraints were shown to hold with equalities, which reduces the search space in the optimization problems. Via numerical examples, performance gains in localization performance and/or power saving were demonstrated, which are due to increased degree of freedom in the proposed optimization problems in comparison to that in Keskin et al. [8]. In particular, electrical power consumption can be reduced by around 45% or localization accuracy can be improved by as much as 25% via the proposed optimal pulse design approach in certain scenarios.

Overall, the main rationale behind the proposed approaches is that under given practical constraints on electrical powers, illumination levels, and/or effective bandwidths, we can design pulse shapes in an optimal manner to maximize the localization accuracy (or, to minimize the energy consumption). It is observed that significant improvements can be achieved in some scenarios by satisfying all the practical constraints. In addition, the proposed optimization problems for the pulse design approaches are convex and they can be solved very rapidly via standard tools. Moreover, the proposed optimization algorithms do not have to be solved very frequently as location updates are not very frequent in indoor localization systems. As an important direction for future work, experiments can be conducted to assess the benefits of the proposed pulse design approaches.

Declaration of Competing Interest

The authors declare that they have no known competing financial interests or personal relationships that could have appeared to influence the work reported in this paper.

Appendix A. FIMs for the VLP system

The (k_1, k_2)th element of the FIM for the asynchronous VLP system model can be expressed as Keskin et al. [35]

$$[\mathbf{J}_{asy}]_{k_1,k_2} = \frac{R_p^2}{\sigma^2} \sum_{i=1}^{N_L} \left(E_2^{(i)} - \frac{(E_3^{(i)})^2}{E_1^{(i)}} \right) \frac{\partial \alpha_i}{\partial l_{r,k_1}} \frac{\partial \alpha_i}{\partial l_{r,k_2}} \tag{52}$$

for $k_1, k_2 \in \{1, 2, 3\}$, with $E_1^{(i)}, E_2^{(i)}$, and $E_3^{(i)}$ being as defined in (5), (6), and (7), respectively.

The (k_1, k_2)th element of the FIM for the synchronous VLP system model can be found as Keskin et al. [35]

$$[\mathbf{J}_{syn}]_{k_1,k_2} = \frac{R_p^2}{\sigma^2} \sum_{i=1}^{N_L} \Bigg[E_2^{(i)} \frac{\partial \alpha_i}{\partial l_{r,k_1}} \frac{\partial \alpha_i}{\partial l_{r,k_2}} + E_1^{(i)} \alpha_i^2 \frac{\partial \tau_i}{\partial l_{r,k_1}} \frac{\partial \tau_i}{\partial l_{r,k_2}}$$
$$- E_3^{(i)} \alpha_i \left(\frac{\partial \alpha_i}{\partial l_{r,k_1}} \frac{\partial \tau_i}{\partial l_{r,k_2}} + \frac{\partial \tau_i}{\partial l_{r,k_1}} \frac{\partial \alpha_i}{\partial l_{r,k_2}} \right) \Bigg] \tag{53}$$

for $k_1, k_2 \in \{1, 2, 3\}$.

With the assumption in Section 3.1 induced, i.e., $E_3^{(i)} = 0$, $i = 1, \ldots, N_L$, the FIMs $\mathbf{J}_{asy}$ and $\mathbf{J}_{syn}$ can be expressed as

$$\mathbf{J}_{asy}(\mathbf{E}_2) = (\mathbf{I}_3 \otimes \mathbf{E}_2)^T \boldsymbol{\Gamma} \tag{54}$$

and

$$\mathbf{J}_{syn}(\mathbf{E}_1, \mathbf{E}_2) = (\mathbf{I}_3 \otimes \mathbf{E}_2)^T \boldsymbol{\Gamma} + (\mathbf{I}_3 \otimes \mathbf{E}_1)^T \widetilde{\boldsymbol{\Gamma}} \tag{55}$$

with

$$\boldsymbol{\Gamma} \triangleq \begin{bmatrix} \boldsymbol{\gamma}_{1,1} & \boldsymbol{\gamma}_{1,2} & \boldsymbol{\gamma}_{1,3} \\ \boldsymbol{\gamma}_{2,1} & \boldsymbol{\gamma}_{2,2} & \boldsymbol{\gamma}_{2,3} \\ \boldsymbol{\gamma}_{3,1} & \boldsymbol{\gamma}_{3,2} & \boldsymbol{\gamma}_{3,3} \end{bmatrix} \in \mathbb{R}^{3N_L \times 3} \tag{56}$$

$$\boldsymbol{\gamma}_{k_1,k_2} \triangleq \left[\gamma_{k_1,k_2}^{(1)}, \ldots, \gamma_{k_1,k_2}^{(N_L)} \right]^T \in \mathbb{R}^{N_L} \tag{57}$$

$$\gamma_{k_1,k_2}^{(i)} \triangleq \frac{R_p^2}{\sigma^2} \frac{\partial \alpha_i}{\partial l_{r,k_1}} \frac{\partial \alpha_i}{\partial l_{r,k_2}}, \quad i = 1, \ldots, N_L \tag{58}$$

$$\widetilde{\boldsymbol{\Gamma}} \triangleq \begin{bmatrix} \widetilde{\boldsymbol{\gamma}}_{1,1} & \widetilde{\boldsymbol{\gamma}}_{1,2} & \widetilde{\boldsymbol{\gamma}}_{1,3} \\ \widetilde{\boldsymbol{\gamma}}_{2,1} & \widetilde{\boldsymbol{\gamma}}_{2,2} & \widetilde{\boldsymbol{\gamma}}_{2,3} \\ \widetilde{\boldsymbol{\gamma}}_{3,1} & \widetilde{\boldsymbol{\gamma}}_{3,2} & \widetilde{\boldsymbol{\gamma}}_{3,3} \end{bmatrix} \in \mathbb{R}^{3N_L \times 3} \tag{59}$$

$$\widetilde{\boldsymbol{\gamma}}_{k_1,k_2} \triangleq \left[\widetilde{\gamma}_{k_1,k_2}^{(1)}, \ldots, \widetilde{\gamma}_{k_1,k_2}^{(N_L)} \right]^T \in \mathbb{R}^{N_L} \tag{60}$$

$$\widetilde{\gamma}_{k_1,k_2}^{(i)} \triangleq \frac{R_p^2}{\sigma^2} \alpha_i^2 \frac{\partial \tau_i}{\partial l_{r,k_1}} \frac{\partial \tau_i}{\partial l_{r,k_2}}, \quad i = 1, \ldots, N_L \tag{61}$$

for $k_1, k_2 \in \{1, 2, 3\}$, where $\mathbf{I}_3$ stands for the 3×3 identity matrix and $\otimes$ denotes the Kronecker product. To compute the values in (58) and (61), we note

$$\frac{\partial \alpha_i}{\partial l_{r,k}} = -\frac{(m_i+1)S}{2\pi} \Bigg(\frac{((\boldsymbol{l}_r - \boldsymbol{l}_t^i)^T \boldsymbol{n}_t^i)^{m_i-1}}{\|\boldsymbol{l}_r - \boldsymbol{l}_t^i\|^{m_i+3}} \left(m_i n_{t,k}^i (\boldsymbol{l}_r - \boldsymbol{l}_t^i)^T \boldsymbol{n}_r + n_{r,k}(\boldsymbol{l}_r - \boldsymbol{l}_t^i)^T \boldsymbol{n}_t^i \right)$$
$$- \frac{(m_i+3)(l_{r,k} - l_{t,k}^i)}{\|\boldsymbol{l}_r - \boldsymbol{l}_t^i\|^{m_i+5}} \left((\boldsymbol{l}_r - \boldsymbol{l}_t^i)^T \boldsymbol{n}_t^i \right)^{m_i} (\boldsymbol{l}_r - \boldsymbol{l}_t^i)^T \boldsymbol{n}_r \Bigg) \tag{62}$$

and

$$\frac{\partial \tau_i}{\partial l_{\mathrm{r},k}} = \frac{l_{\mathrm{r},k} - l_{\mathrm{t},k}^i}{c \| \boldsymbol{l}_\mathrm{r} - \boldsymbol{l}_\mathrm{t}^i \|} \tag{63}$$

for $i = 1, \ldots, N_\mathrm{L}$ and $k = 1, 2, 3$ [35].

CRediT authorship contribution statement

Onurcan Yazar: Methodology, Formal analysis, Software, Writing – original draft. **Sinan Gezici:** Conceptualization, Methodology, Writing – original draft, Writing – review & editing, Supervision.

References

[1] J. Armstrong, Y.A. Sekercioglu, A. Neild, Visible light positioning: a roadmap for international standardization, IEEE Commun. Mag. 51 (12) (2013) 68–73.

[2] T. Komine, M. Nakagawa, Fundamental analysis for visible-light communication system using LED lights, IEEE Trans. Consum. Electron. 50 (1) (2004) 100–107.

[3] Z. Ghassemlooy, L.N. Alves, S. Zvanovec, M.A. Khalighi, Visible Light Communications: Theory and Applications, CRC Press, 2017.

[4] L. Feng, R.Q. Hu, J. Wang, P. Xu, Y. Qian, Applying VLC in 5G networks: architectures and key technologies, IEEE Netw. 30 (6) (2016) 77–83.

[5] G. Blinowski, Security issues in visible light communication systems, in: 13th IFAC and IEEE Conference on Programmable Devices Embedded Systems, 2015, pp. 234–239.

[6] M. Katz, I. Ahmed, Opportunities and challenges for visible light communications in 6G, in: 2nd 6G Wireless Summit, Levi, Finland, 2020, pp. 1–5.

[7] M. Giordani, M. Polese, M. Mezzavilla, S. Rangan, M. Zorzi, Toward 6G networks: use cases and technologies, IEEE Commun. Mag. 58 (3) (2020) 55–61.

[8] M.F. Keskin, A.D. Sezer, S. Gezici, Optimal and robust power allocation for visible light positioning systems under illumination constraints, IEEE Trans. Commun. 67 (1) (2019) 527–542.

[9] T.Q. Wang, Y.A. Sekercioglu, A. Neild, J. Armstrong, Position accuracy of time-of-arrival based ranging using visible light with application in indoor localization systems, J. Lightwave Technol. 31 (20) (2013) 3302–3308.

[10] P. Du, S. Zhang, C. Chen, A. Alphones, W. Zhong, Demonstration of a low–complexity indoor visible light positioning system using an enhanced TDOA scheme, IEEE Photonics J. 10 (4) (2018) 1–10.

[11] X. Sun, Y. Zou, J. Duan, A. Shi, The positioning accuracy analysis of AOA-based indoor visible light communication system, in: 2015 International Conference on Optoelectronics and Microelectronics, Changchun, China, 2015, pp. 186–190.

[12] A. Naz, H.M. Asif, T. Umer, B.S. Kim, PDOA based indoor positioning using visible light communication, IEEE Access 6 (2018) 7557–7564.

[13] K. Majeed, S. Hranilovic, Performance bounds on passive indoor positioning using visible light, J. Lightwave Technol. 38 (8) (2020) 2190–2200. Apr. 15

[14] H. Hosseinianfar, M. Brandt-Pearce, Performance limits for fingerprinting-based indoor optical communication positioning systems exploiting multipath reflections, IEEE Photonics J 12 (4) (2020) 1–16.

[15] B. Zhou, A. Liu, V. Lau, Performance limits of visible light-based user position and orientation estimation using received signal strength under NLOS propagation, IEEE Trans. Wirel. Commun. 18 (11) (2019) 5227–5241.

[16] T. Tanaka, S. Haruyama, New position detection method using image sensor and visible light LEDs, in: Second International Conference on Machine Vision, 2009, pp. 150–153.

[17] M. Yoshino, S. Haruyama, M. Nakagawa, High-accuracy positioning system using visible LED lights and image sensor, in: IEEE Radio and Wireless Symposium, 2008, pp. 439–442.

[18] T.H. Do, M. Yoo, Analysis on visible light communication using rolling shutter CMOS sensor, in: International Conference on Information and Communication Technology Convergence (ICTC), 2015, pp. 755–757.

[19] W.A. Cahyadi, Optical camera communications: principles, modulations, potential and challenges, Electronics 9 (9) (2020) 1339.

[20] B. Lin, et al., Experimental demonstration of an indoor positioning system based on artificial neural network, Opt. Eng. 58 (1) (2019) 016104.

[21] C. Hsu, et al., Accurate indoor visible light positioning system utilizing machine learning technique with height tolerance, in: Optical Fiber Communications Conference and Exposition (OFC), 2018.

[22] Y.-C. Chuang, et al., Visible light communication and positioning using positioning cells and machine learning algorithms, Opt. Express 27 (2019) 16377–16383.

[23] O. Yazar, M.F. Keskin, S. Gezici, Power-efficient positioning for visible light systems via chance constrained optimization, IEEE Trans. Aerosp. Electron. Syst. 56 (5) (2020) 4124–4131.

[24] D. Bykhovsky, S. Arnon, Multiple access resource allocation in visible light communication systems, J. Lightwave Technol. 32 (8) (2014) 1594–1600. Apr. 15

[25] X. Ling, J. Wang, X. Liang, Z. Ding, C. Zhao, Offset and power optimization for DCO-OFDM in visible light communication systems, IEEE Trans. Signal Process. 64 (2) (2016) 349–363.

[26] H. Yang, Reinforcement learning-based intelligent resource allocation for integrated VLCP systems, IEEE Wirel. Commun. Lett. 8 (4) (2019) 1204–1207.

[27] H. Yang, Resource allocation for multi-user integrated visible light communication and positioning systems, in: 2019 IEEE International Conference on Communications, Shanghai, China, 2019, pp. 1–6.

[28] H. Yang, Coordinated resource allocation-based integrated visible light communication and positioning systems for indoor iot, IEEE Trans. Wirel. Commun. 19 (7) (2020) 4671–4684.

[29] N. Garcia, A.M. Haimovich, M. Coulon, M. Lops, Resource allocation in MIMO radar with multiple targets for non-coherent localization, IEEE Trans. Signal Process. 62 (10) (2014) 2656–2666. May. 15

[30] T. Zhang, C. Qin, A.F. Molisch, Q. Zhang, Joint allocation of spectral and power resources for non-cooperative wireless localization networks, IEEE Trans. Commun. 64 (9) (2016) 3733–3745.

[31] W. Li, T. Zhang, Y. Shen, A.F. Molisch, Q. Zhang, Robust resource allocation in wireless localization networks, in: 2014 IEEE/CIC International Conference on Communications in China, Shanghai, China, 2014, pp. 442–447.

[32] T. Nowak, System and signal design for an energy-efficient multi-frequency localization system, in: 2014 IEEE Topical Conference on Wireless Sensors and Sensor Networks, Newport Beach, CA, USA, 2014, pp. 55–57.

[33] J.M. Kahn, J.R. Barry, Wireless infrared communications, Proc. IEEE 85 (2) (1997) 265–298.

[34] H.V. Poor, An Introduction to Signal Detection and Estimation, Springer-Verlag, New York, NY, USA, 1994.

[35] M.F. Keskin, S. Gezici, O. Arikan, Direct and two-step positioning in visible light systems, IEEE Trans. Commun. 66 (1) (2018) 239–254.

[36] Y. Qi, H. Kobayashi, H. Suda, Analysis of wireless geolocation in a non–line-of-sight environment, IEEE Trans. Wirel. Commun. 5 (3) (2006) 672–681.

[37] Y. Qi, Wireless Geolocation in a Non-Line-of-Sight Environment, Princeton University, 2003 Ph.D. Dissertation.

[38] C. Gong, S. Li, Q. Gao, Z. Xu, Power and rate optimization for visible light communication system with lighting constraints, IEEE Trans. Signal Process. 63 (16) (2015) 4245–4256.

[39] J. Gancarz, H. Elgala, T.D.C. Little, Impact of lighting requirements on VLC systems, IEEE Commun. Mag. 51 (12) (2013) 34–41.

[40] A. Pandharipande, D. Caicedo, Adaptive illumination rendering in LED lighting systems, IEEE Trans. Syst., Man, Cybern. 43 (5) (2013) 1052–1062.

[41] A. Oppenheim, A. Willsky, S. Nawab, Signals and Systems, Prentice Hall, Upper Saddle River, NJ, USA, 1997.

[42] S. Boyd, L. Vandenberghe, Convex Optimization, Cambridge Univ. Press, Cambridge, U.K., 2004.

[43] G.H. Golub, C.F. Van Loan, Matrix Computations, Johns Hopkins, Baltimore, MD, USA, 1996.

Onurcan Yazar received the B.S. degree in Electrical and Electronics Engineering from Bilkent University, Turkey, in 2019. He is currently working toward the M.S. degree in Electrical and Electronics Engineering at Bilkent University. His research interests include signal processing, wireless localization, and visible light communications.

Sinan Gezici received the B.S. degree from Bilkent University, Turkey in 2001, and the Ph.D. degree in Electrical Engineering from Princeton University in 2006. From 2006 to 2007, he worked at Mitsubishi Electric Research Laboratories, Cambridge, MA. Since 2007, he has been with the Department of Electrical and Electronics Engineering at Bilkent University, where he is currently a Professor. Dr. Gezici's research interests are in the areas of detection and estimation theory, wireless communications, and localization systems. Among his publications in these areas is the book Ultra-wideband Positioning Systems: Theoretical Limits, Ranging Algorithms, and Protocols (Cambridge University Press, 2008). Dr. Gezici was an associate editor for IEEE Transactions on Communications, IEEE Wireless Communications Letters, and Journal of Communications and Networks.